

# Novel Small-Molecule Inhibitor of NLRP3 Inflammasome Reverses Cognitive Impairment in an Alzheimer's Disease Model

Muhammad Haseeb,<sup>II</sup> Nasir Javaid,<sup>II</sup> Farzana Yasmineen, Uisuk Jeong, Ji Hye Han, Juhwan Yoon, Jee Yeon Seo, Jae Kyung Heo, Ho Chul Shin, Moon Suk Kim, Wook Kim,\* and Sangdun Choi\*



Cite This: *ACS Chem. Neurosci.* 2022, 13, 818–833



Read Online

ACCESS |

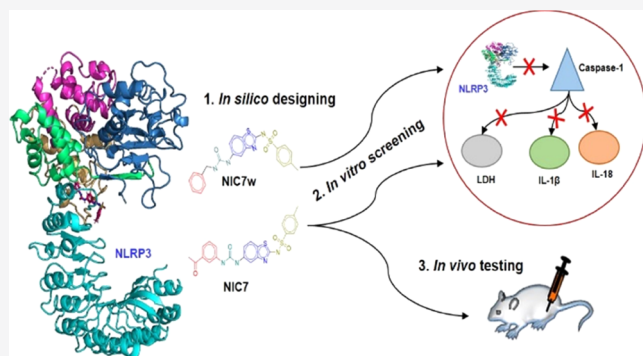
Metrics & More

Article Recommendations

Supporting Information

**ABSTRACT:** Aberrant activation of the Nod-like receptor family pyrin domain-containing 3 (NLRP3) inflammasome plays an essential role in multiple diseases, including Alzheimer's disease (AD) and psoriasis. We report a novel small-molecule inhibitor, NLRP3-inhibitory compound 7 (NIC7), and its derivative, which inhibit NLRP3-mediated activation of caspase 1 along with the secretion of interleukin (IL)-1 $\beta$ , IL-18, and lactate dehydrogenase. We examined the therapeutic potential of NIC7 in a disease model of AD by analyzing its effect on cognitive impairment as well as the expression of dopamine receptors and neuronal markers. NIC7 significantly reversed the associated disease symptoms in the mice model. On the other hand, NIC7 did not reverse the disease symptoms in the imiquimod (IMQ)-induced disease model of psoriasis. This indicates that IMQ-based psoriasis is independent of NLRP3. Overall, NIC7 and its derivative have therapeutic prospects to treat AD or NLRP3-mediated diseases.

**KEYWORDS:** NLRP3, inflammasome, small-molecule inhibitor, virtual screening, Alzheimer's disease



Downloaded via AJOU UNIV on October 26, 2023 at 11:07:18 (UTC).  
See https://pubs.acs.org/sharingguidelines for options on how to legitimately share published articles.

## INTRODUCTION

Inflammasomes are multiprotein complexes of the innate immune system that detect pathogens via pattern recognition receptors and are responsible for the activation of inflammatory responses.<sup>1</sup> The core components of the inflammasome are nucleotide-binding oligomerization domain (NOD)-like receptors (NLRs), absent in melanoma 2 (AIM2)-like receptors, pyrin receptors, and an enzymatic component (caspase 1). In addition to these components, most inflammasomes contain an adaptor protein named apoptosis-associated speck-like protein containing a caspase activation and recruitment domain (ASC).<sup>2</sup> To date, several types of inflammasome have been reported, such as NLR pyrin domain-containing (NLRP1, NLRP2, NLRP3, NLRP6, NLRP7, and NLRP12), NLR family CARD domain-containing protein 4 (NLRC4), and interferon-inducible protein 16 (IFI16).<sup>3,4</sup>

NLRP3, the most widely studied inflammasome type, has been implicated in several complex diseases of the central nervous system.<sup>5,6</sup> The core component of the NLRP3 scaffold consists of CARD (ASC) and a precursor enzyme: procaspase 1. Upon sensing danger stimuli, NLRP3 binds to ASC and interacts with cysteine protease caspase 1 to assemble the inflammasome. This event results in caspase 1 activation and subsequent maturation and secretion of proinflammatory cytokines IL-1 $\beta$  and IL-18.<sup>7</sup> In addition, caspase 1 activation can mediate the death of cells, either directly (via a process

known as pyroptosis) or indirectly (through apoptosis).<sup>8</sup> Besides the canonical NLRP3 inflammasome, the noncanonical NLRP3 inflammasome is another developing area of interest; the latter type is formed by caspase 11 in mice. Humans do not have caspase 11, and recent reports suggest that its orthologs in human cells are caspases 4 and 5, which play a similar role.<sup>2,9</sup> NLRP3 inflammasome activation can also be implemented through several cellular mechanisms and cytoskeletal signatures. Recent studies have identified NIMA-related kinase 7 (NEK7) as a new regulator of the NLRP3 inflammasome; NEK7 is a protein involved in cell cycle progression. Upon interaction of NEK7 with the leucine-rich repeat (LRR) domain of NLRP3, it activates the NLRP3 inflammasome independently of its kinase activity.<sup>10</sup> The latest developments have significantly improved our knowledge about the molecular mechanisms by which various inflammasomes are activated and about their involvement in the initiation or progression of diseases.<sup>2</sup> In addition, NLRP3 plays a part in several autoimmune and autoinflammatory diseases, including

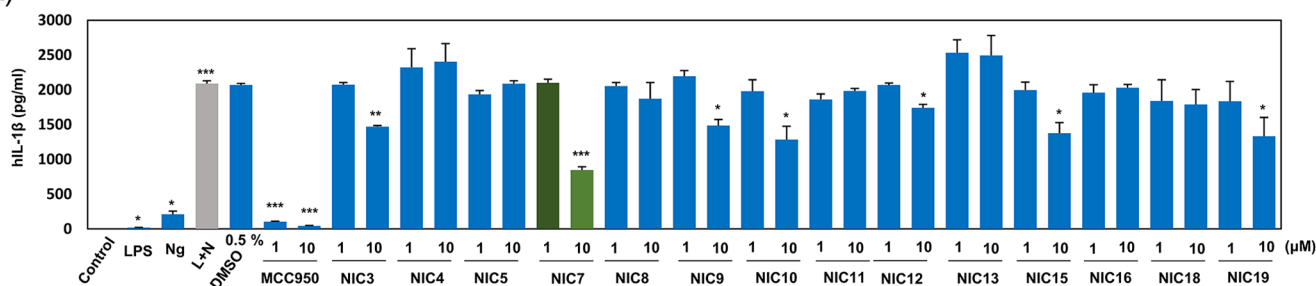
Received: December 17, 2021

Accepted: February 15, 2022

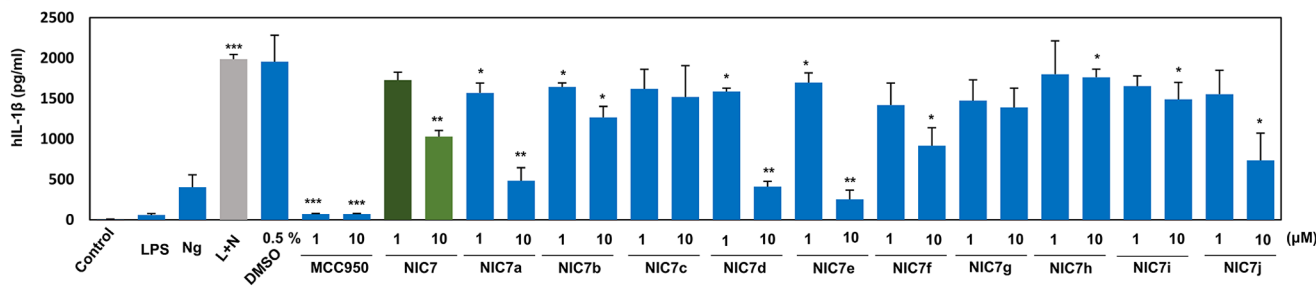
Published: February 24, 2022



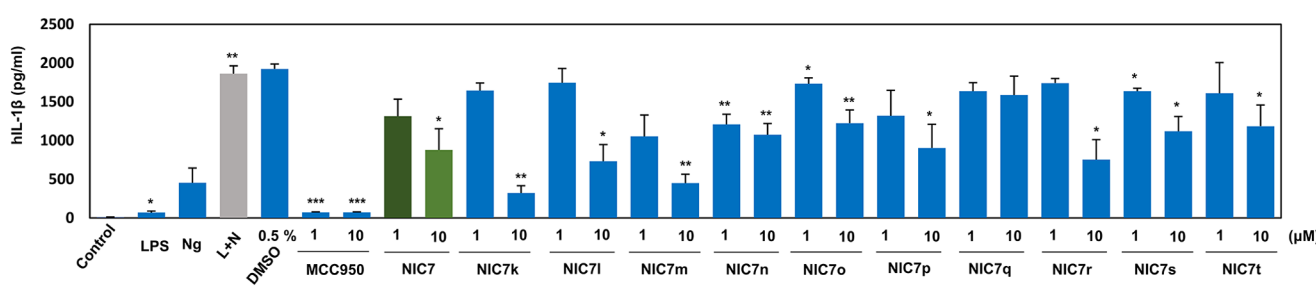
(A)



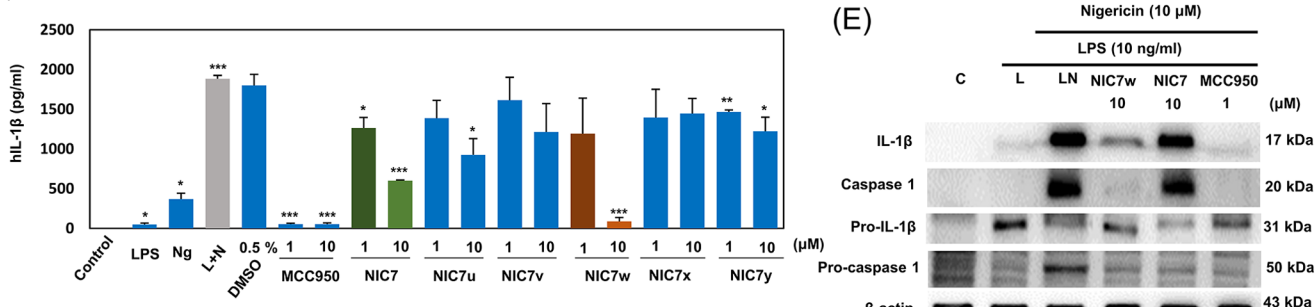
(B)



(C)



(D)



(E)

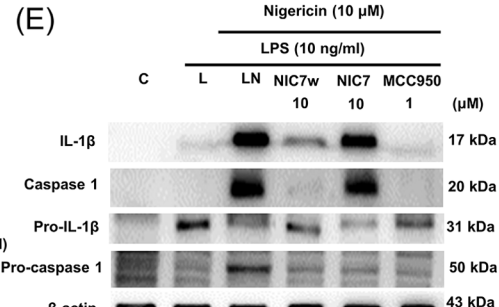


**Figure 1.** Functional screening of NLRP3 inhibitors. (A–D) NLRP3 inhibition by nontoxic compounds was evaluated by checking the secretion level of human-IL-1 $\beta$  (hIL-1 $\beta$ ). PMA-differentiated THP-1 cells were primed with LPS (10 ng/mL) for 4 h followed by treatment with (A) potential leads and (B–D) derivatives of NIC7 (1 and 10  $\mu\text{M}$ ) for 1 h. NLRP3 was activated with nigericin (10  $\mu\text{M}$ ) for 1 h, and the supernatant was collected to measure the level of human interleukin (IL)-1 $\beta$  with the respective enzyme-linked immunosorbent assay (ELISA) kit. The presented data are the average of three independent experiments, where each experiment was conducted in duplicate, and statistical analysis was performed by two-tailed paired Student's *t*-test (\* $P < 0.05$ , \*\* $P < 0.01$ , and \*\*\* $P < 0.001$ ). (E) The inhibition of the NLRP3-signaling pathway by NIC7w, NIC7, and MCC950 was evaluated by western blotting. The total protein was extracted from all samples and immunoblotted with respective antibodies. The  $\beta$ -actin served as an internal control. Nigericin: Ng; LPS + Nigericin: L + N.

metabolic disorders (obesity, gout, type 2 diabetes mellitus, and atherosclerosis) and neurodegenerative diseases (Alzheimer's disease [AD], traumatic brain injury, multiple sclerosis, and Parkinson's disease).<sup>11,12</sup>

The participation of the NLRP3 inflammasome in the development of AD has been demonstrated in transgenic (APP/PS1) mice that show chronic amyloid- $\beta$  (A $\beta$ ) deposition with caspase 1 and NLRP3 deficiency. These

mice feature decreased secretion of A $\beta$  as well as cognitive dysfunction and neuroinflammation. The expression of caspase 1 in the brain of AD patients has been reported too, indicating a correlation between inflammasome activation and AD in humans.<sup>13</sup> The development of AD leads to the deterioration of memory in AD models. The spatial learning and memory deficits are being commonly monitored in AD models using the Morris water maze<sup>14–19</sup> or Y-maze test.<sup>20–23</sup> Nonetheless,

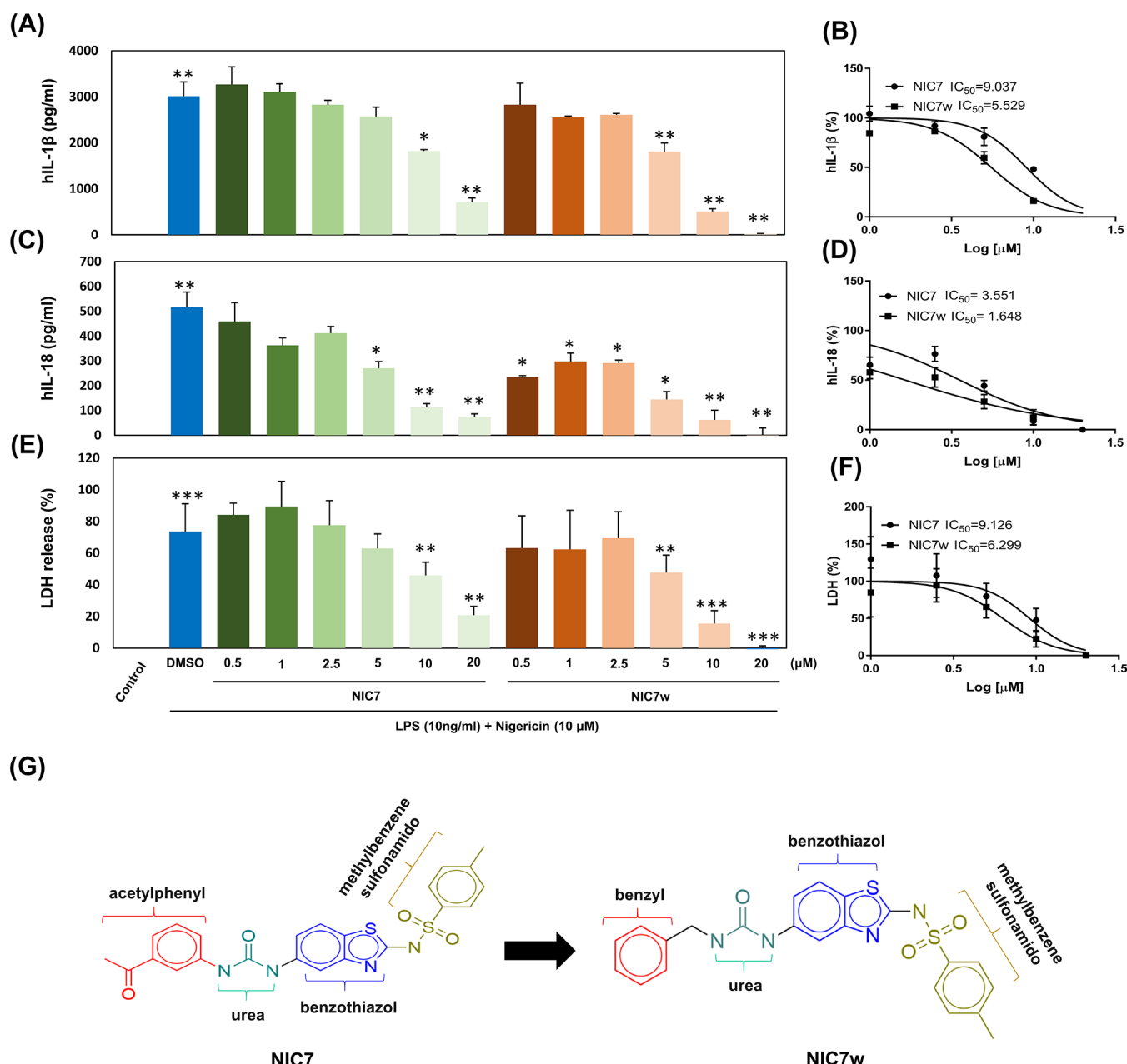


**Figure 2.**  $IC_{50}$  determination for NIC7 and NIC7w. (A–F) Various concentrations of NIC7 and NIC7w were applied, samples were collected and processed to determine the inhibition of (A, B) human interleukin (IL)-1 $\beta$ , (C, D) human-IL-18, and (E, F) lactate dehydrogenase (LDH) with respective kits. The obtained numerical values were used to calculate the  $IC_{50}$  values by GraphPad Prism 7 software. The presented data are the average of three independent experiments, where statistical analysis was performed by two-tailed paired Student's *t*-test (\* $P < 0.05$ , \*\* $P < 0.01$ , \*\*\* $P < 0.001$ ). (G) A two-dimensional chemical structure of NIC7 and NIC7w.

deficits in learning and memory can be evaluated using the novel object recognition (NOR) test.<sup>24–31</sup> Therefore, these studies mean that the NLRP3 inflammasome is a potential target for the treatment of neuroinflammation and AD. Several biologic therapeutics—including antibodies canakinumab, anakinra, and rilonacept—target inflammasome effectors IL-1 $\beta$ , IL-1RA, and IL-18 for the treatment of NLRP3-related diseases.<sup>32,33</sup> Several small-molecule inhibitors of the NLRP3 inflammasome have been reported, including glyburide, parthenolide, Bay 11-7082, auranofin, CRID3, and  $\beta$ -hydroxybutyrate (BHB), although some of these inhibitors are nonspecific and have rather limited potency.<sup>34–38</sup> Furthermore, MCC950 has recently been identified as a highly

selective NLRP3 inflammasome inhibitor that blocks both canonical and noncanonical NLRP3 inflammasomes at nanomolar concentrations.<sup>39</sup> In another study, a small-molecule NLRP3 inhibitor, JC-124, was identified and tested against AD-related deficits in transgenic mice (strain TgCRND8).<sup>40</sup> Collectively, these data support the development of NLRP3 inflammasome inhibitors as a potential treatment of AD.

In this study, we identified a novel NLRP3 inflammasome inhibitor, i.e., a small-molecule agent referred to below as NLRP3-inhibitory compound 7 (NIC7), and its potent derivative NIC7w. Through rational design, our novel compounds NIC7 and NIC7w demonstrated selective inhibition of the NLRP3 inflammasome and activation of

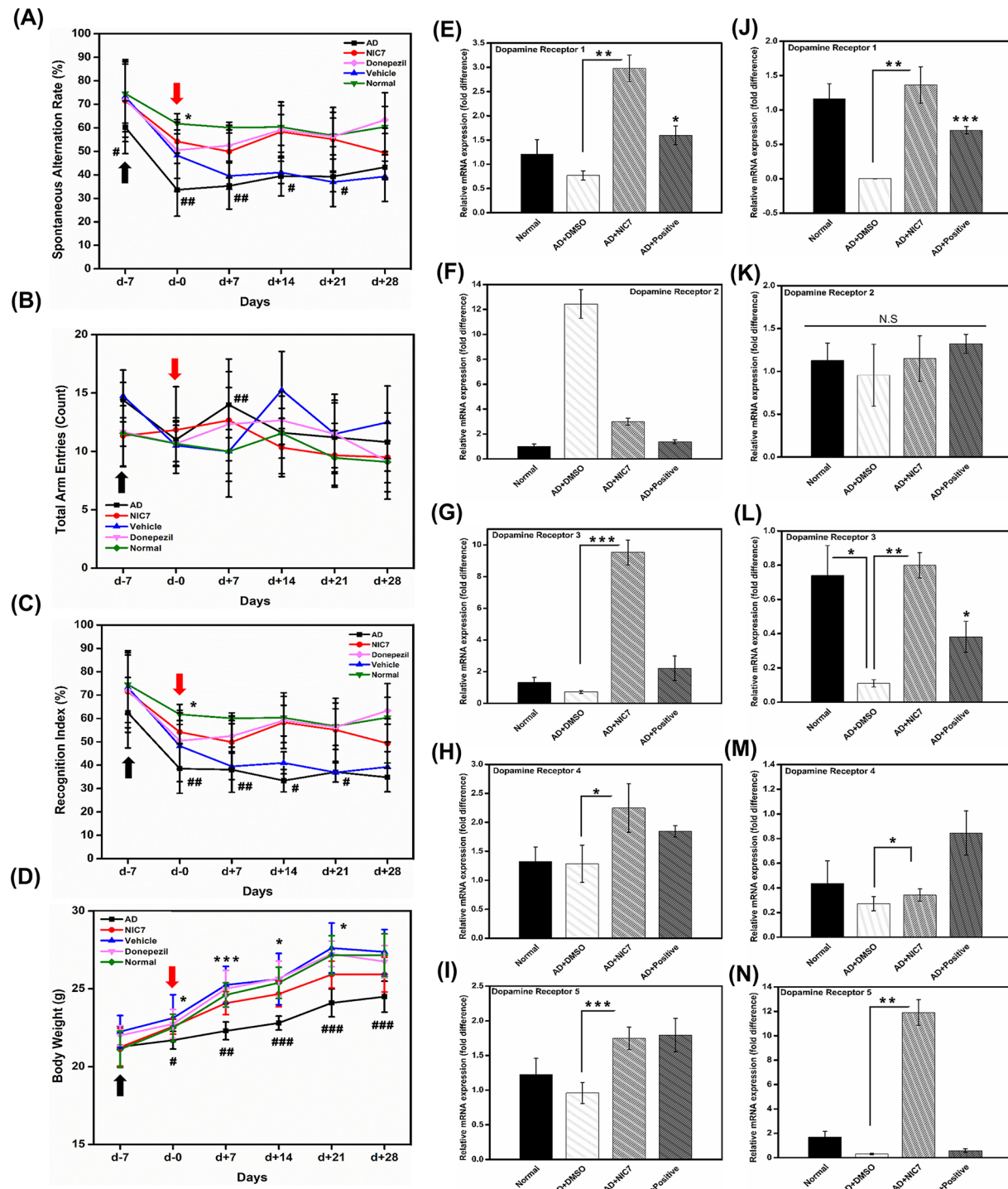


**Figure 3.** Recovery from cognitive impairment in the Alzheimer's disease (AD) model. The AD model was set up by injection of  $\text{A}\beta_{42}$  (black arrow) seven days prior (d-7) to intraperitoneal injection of NIC7 (100 nmol/g), donepezil (1 mg/kg), or dimethyl sulfoxide (DMSO) as a vehicle (1%) (d-0; red arrow) for 3 days/week. (A, B) Spatial working memory was evaluated in each group ( $n = 6$ ) in terms of the (A) spontaneous alternation rate by the Y-maze test and (B) total arm entries. (C) Recognition memory was evaluated by the novel object recognition test, and the data are presented as a percentage of the recognition rate for each group. (D) Body weight in each group was measured at the indicated time points. Values are expressed as means  $\pm$  scanning electron microscopy (SEM).  $\#p < 0.05$ ,  $\#\#p < 0.01$ , and  $\#\#\#p < 0.001$  vs the normal group, and  $*p < 0.05$ ,  $**p < 0.01$ , and  $***p < 0.001$  vs the AD group (Student's *t*-test). (E–N) Mice were sacrificed after 28 days of treatment (d+28), and the brain tissues were used to measure the expression level of dopamine receptors (1–5) in the (E–I) cerebral cortex and (J–N) hippocampus regions by real-time quantitative polymerase chain reaction (PCR). The values were normalized to  $\beta$ -actin. The presented data is the average of three experiments and statistical analysis was performed using Student's *t*-test (\* $P < 0.05$ , \*\* $P < 0.01$ , and \*\*\* $P < 0.001$ ), N.S.: Nonspecific.

caspase 1, IL-1 $\beta$ , and IL-18. Treatment of AD C57BL/6 mice with NIC7 significantly improved several AD symptoms such as inflammatory responses, neuronal marker levels, and

cognitive parameters. We hypothesize that the NLRP3 inflammasome, which is generated after AD, is implicated in the progression of cognitive impairment and neuronal tissue

damage. Thus, targeting NLRP3 inflammasome with our novel compound will have a protective impact and imply potential therapeutic effects against a variety of inflammasome-related diseases.

## RESULTS

**Identification of NIC7 as a Potential Lead against NLRP3 Signaling.** So far, the experimental crystal structure of NLRP3 bound to a small-molecule ligand is unavailable in the PDB. Initially, the identification of a novel small-molecule inhibitor of NLRP3 (NIC7) was carried out through an *in silico* approach using the cryo-EM structure of the NLRP3–NEK7 complex (PDB ID: 6NPY)<sup>41</sup> and a multifunctional library of over 28 million commercially available chemical compounds (Table S1 and Figure S1). Compounds having drug-like physicochemical properties were isolated using a fingerprint-based similarity metric Tanimoto coefficient (TC) with the selected NLRP3 inhibitors as reference molecules (Table S2). The resulting set of 367 328 ligands was then screened in accordance with pharmacophore models of the reference ligands, which have well-defined intermolecular interactions with NLRP3. Next, the resultant set of 70 040 ligands was subjected to structure-based virtual screening on sites I and II of NLRP3. The docked ligand poses were ranked by MMFF94x force field-based binding free energy (GBVI/WSA dG) scores. After close visual inspection of the top ~200 virtual hits (from multiple rounds of docking) for their potential fit into the site I and site II pockets of NLRP3 (Figure S2), 19 top-scoring consensus ligands (designated as NIC1–NIC19) were experimentally validated to assess their inhibitory activity.

First, we evaluated their cytotoxicity on phorbol 12-myristate 13-acetate (PMA)-differentiated human monocytic cells (THP-1) by treating them (at 10 or 50  $\mu$ M) for 24 h. Of the 19 compounds, NIC1, -2, -6, -14, and -17 showed significant toxicity at higher concentrations (Figures S3A,B). The remaining compounds were tested for their potential to inhibit the NLRP3-driven secretion of IL-1 $\beta$ . For this purpose, we primed PMA-differentiated THP-1 cells with lipopolysaccharide (LPS), a Toll-like receptor 4 (TLR4) ligand, and activated NLRP3 with nigericin after treating with tested compounds as well as control, MCC950.<sup>39</sup> Among all of the compounds, NIC7 showed the highest potency in inhibiting the IL-1 $\beta$  secretion (Figure 1A). Therefore, NIC7 was selected as an appropriate lead to design its derivatives to improve the activity.

**NIC7w Shows Greater Potency than NIC7.** Next, by structural modifications, we aimed to improve the inhibitory effect of the primary lead, NIC7, against the NLRP3-signaling pathway. We searched for commercially available NIC7 derivatives in the MolPort database (<https://www.molport.com/shop/index>) and found 100 promising distinct derivatives that are structurally similar to the NIC7 main scaffold with various functional groups attached. The derivatives were first computationally docked into site I and site II of NLRP3 by means of the docked pose of NIC7 as a template and were ranked by their binding-affinity score (see **Structure-Based Virtual Screening**). The top 25 derivatives (referred to as NIC7a–NIC7y) that scored better than NIC7 and showed maximum interactions within 4.5 Å were selected to test their NLRP3-inhibiting potential.

All of the derivatives were first evaluated for their toxicity to THP-1 macrophages at concentrations of 10 and 50  $\mu$ M. None

of the molecules showed significant toxicity to the cells at the highest concentration tested (Figure S3C,D). Therefore, all of the compounds were screened to determine their inhibitory potential toward NLRP3. We followed the same process as mentioned above and analyzed the secretion level of human-IL-1 $\beta$  by the ELISA. Compared to the other compounds, NIC7w caused significantly stronger inhibition at its highest concentration (Figure 1D). We chose NIC7w along with NIC7 and MCC950 (control) to further analyze the inhibition of the NLRP3-signaling pathway using western blot analysis. We observed reduced activation for the key components of the NLRP3-signaling pathway, i.e., IL-1 $\beta$  and caspase 1 (Figure 1E).

The potency of NIC7 and NIC7w was further compared by the calculation of their IC<sub>50</sub> values (half-maximal inhibitory concentrations) in relation to the secretion of IL-1 $\beta$ , IL-18, and lactate dehydrogenase (LDH). By following the above protocol, we applied various concentrations of NIC7 and NIC7w to THP-1 cells and examined the effects. Both NIC7 and NIC7w inhibited the secretion of IL-1 $\beta$  in a concentration-dependent manner with IC<sub>50</sub> of 9.0 and 5.5  $\mu$ M, respectively (Figure 2A,B). Similarly, NIC7 and NIC7w inhibited the secretion of IL-18 in a concentration-dependent manner with IC<sub>50</sub> of 3.5 and 1.6  $\mu$ M, respectively (Figure 2C,D). Additionally, NIC7 and NIC7w inhibited the release of LDH in a concentration-dependent manner with IC<sub>50</sub> values of 9.1 and 6.3  $\mu$ M, respectively (Figure 2E,F). These results indicate that NIC7w is almost twice as effective as NIC7 in inhibiting the NLRP3-signaling pathway. On the other hand, we did not observe any inhibition in the secretion of human-TNF- $\alpha$  and IL-8 (Figure S4). This confirms that NIC7 and NIC7w specifically inhibit the activation of NLRP3 but not the priming step required to produce proinflammatory cytokines (such as TNF- $\alpha$ ) as well as pro-forms of IL-1 $\beta$  and IL-18.

**NIC7 Prevents Memory Impairment in the AD Model.** NLRP3 is reported to be associated with various hippocampal neurodegenerative diseases, including AD.<sup>40</sup> We evaluated the possible reversal of a memory decline by our NLRP3 inflammasome inhibitor, NIC7. In this regard, we examined spatial working memory in the Y-maze test on the mouse model of AD and calculated the spontaneous alternation rate using total arm entries (Figure 3A,B). We confirmed that the NIC7-treated mice spent more time in the novel arm, just as donepezil-treated mice did, in comparison with vehicle-treated and untreated mice (Figure 3A). Considering the involvement of the hippocampus in recognition memory in addition to spatial working memory, we also conducted the novel object recognition test.<sup>42</sup> We found a better recognition index in NIC7- and donepezil-treated mice than in vehicle-treated or untreated mice (Figure 3C). The treatment of NIC7 also helped AD mice in recovering the weight loss during disease (Figure 3D).

The occurrence of AD in patients led to the marked reduction in the expression of components of the dopaminergic system, including dopamine receptors, acetylcholine, and glutamate, in the hippocampus and cerebral cortex.<sup>43–45</sup> To evaluate the effect of NIC7, we sacrificed the mice after 4 weeks of treatment (d+28) and analyzed the mRNA expression level of dopamine receptors (1–5) in the tissue samples of the cerebral cortex and hippocampus. We found significant recovery in the expression of most of the dopamine receptors lost during AD with the treatment of NIC7 (Figure 3E–N).

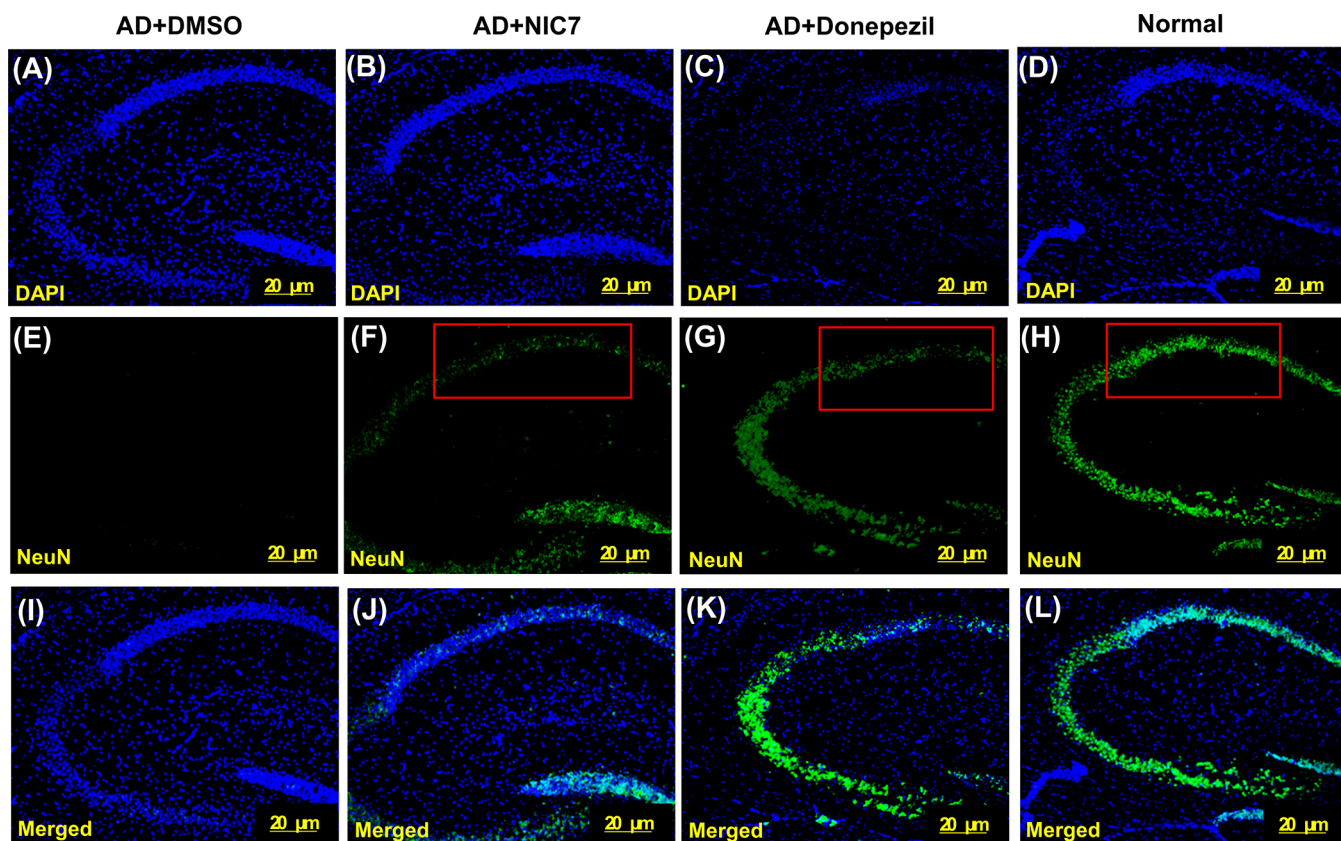


**Figure 4.** Immunohistochemical analysis of a neuronal regeneration marker. (A–L) Neuronal regeneration was assessed by immunohistochemical staining of the hippocampal cryosection for the regeneration marker, NeuN. There were neural impairments in the CA1 region of the AD model, and there was overexpression of NeuN in the donepezil and NIC7 groups (red box). The nuclei were stained with DAPI. (Scale bar = 20  $\mu$ m).

The presence of NLRP3 components in neurons indicates a neurodegenerative role by activated NLRP3 in AD.<sup>46–49</sup> The neurodegeneration leads to the reduction in the neuronal cells and hence its marker, NeuN.<sup>46</sup> To evaluate the effect of NIC7 on neurogenesis in the AD model, we sacrificed the mice after 4 weeks of treatment (d+28) and performed immunohistochemical staining with the antibody specific to the neuronal marker, NeuN. The NIC7 treatment recovered the lost expression of NeuN in the CA1 region of the hippocampus just like donepezil (positive control; Figure 4A–L). These results indicate the potential of NIC7 to reverse NLRP3-mediated cognitive impairment and neurodegeneration in AD.

**Lack of a Benefit of NIC7 in the Mouse Model of Imiquimod (IMQ)-Induced Psoriasis.** Psoriasis is an immune-system-mediated chronic inflammatory skin disease characterized by increased epidermal cell proliferation and differentiation as well as inflammatory cell infiltration into skin lesions.<sup>50</sup> NLRP3 inflammasomes are widely activated in skin inflammatory diseases, and recent research indicates that NLRP3 is genetically associated with psoriasis and that psoriasis patients have greater plasma levels of inflammasome-generated IL-1 $\beta$  and IL-18.<sup>51–53</sup> Nonetheless, some studies have shown that the inflammation induced by IMQ is independent of the NLRP3 inflammasome, and IMQ is capable of inducing inflammation in P2X7 receptor knockout (P2X7R<sup>-/-</sup>) mice.<sup>52,54,55</sup> To test whether NIC7 is effective against IMQ-induced psoriasis, we induced psoriasis symptoms in 6- to 7-week-old C57BL/6 mice by the topical application of 62.5 mg of IMQ cream to their back skin for 4 consecutive days (Figure 5A) along with the administration of NIC7 (124

nmol per gram of mice weight). Comparative analysis revealed that NIC7 did not reduce the psoriasis-mediated skin lesions (Figure 5B), psoriasis area and severity index (PASI) score (Figure 5C), spleen weight (Figure 5D), and loss in body weight (Figure 5E). Next, we assessed histopathological changes in the skin by H&E staining and found no significant alteration in the thickness of the epidermis with the treatment of NIC7 (Figure 5F,G). Collectively, our results are consistent with previous findings suggesting that the model of IMQ-induced psoriasis does not mainly involve NLRP3, which hinders the reversal of disease conditions with our NLRP3-specific inhibitor, NIC7.<sup>52,54,55</sup> It is also reported that the P2X7 receptor signaling is involved in the rIL-23 model to induce NLRP3-dependent psoriasis.<sup>55</sup>

**Stability and Binding Mode of NIC7 and NIC7w.** We checked the stability of both complexes NLRP3–NIC7 and NLRP3–NIC7w as a function of simulation time. The radius of gyration ( $R_g$ ) values indicated that both complexes maintained stability and compactness. However, NLRP3–NIC7 showed an elevated  $R_g$  value of around 3.5–4 nm between 30 and 55 ns and then remained stable throughout the simulation (Figure 6A). The root mean square deviation (RMSD) of the backbone atoms showed that both complexes reached an equilibrium state shortly after ~55 ns of simulation (Figure 6B). In comparison to NIC7, NIC7w has a larger number of hydrogen bonds, especially around 50 ns (Figure 6C). Similarly, the ligand RMSD of both ligands remains stable throughout the simulation, with the exception of NIC7, which fluctuates between 30 and 55 ns before stabilizing (Figure 6D).

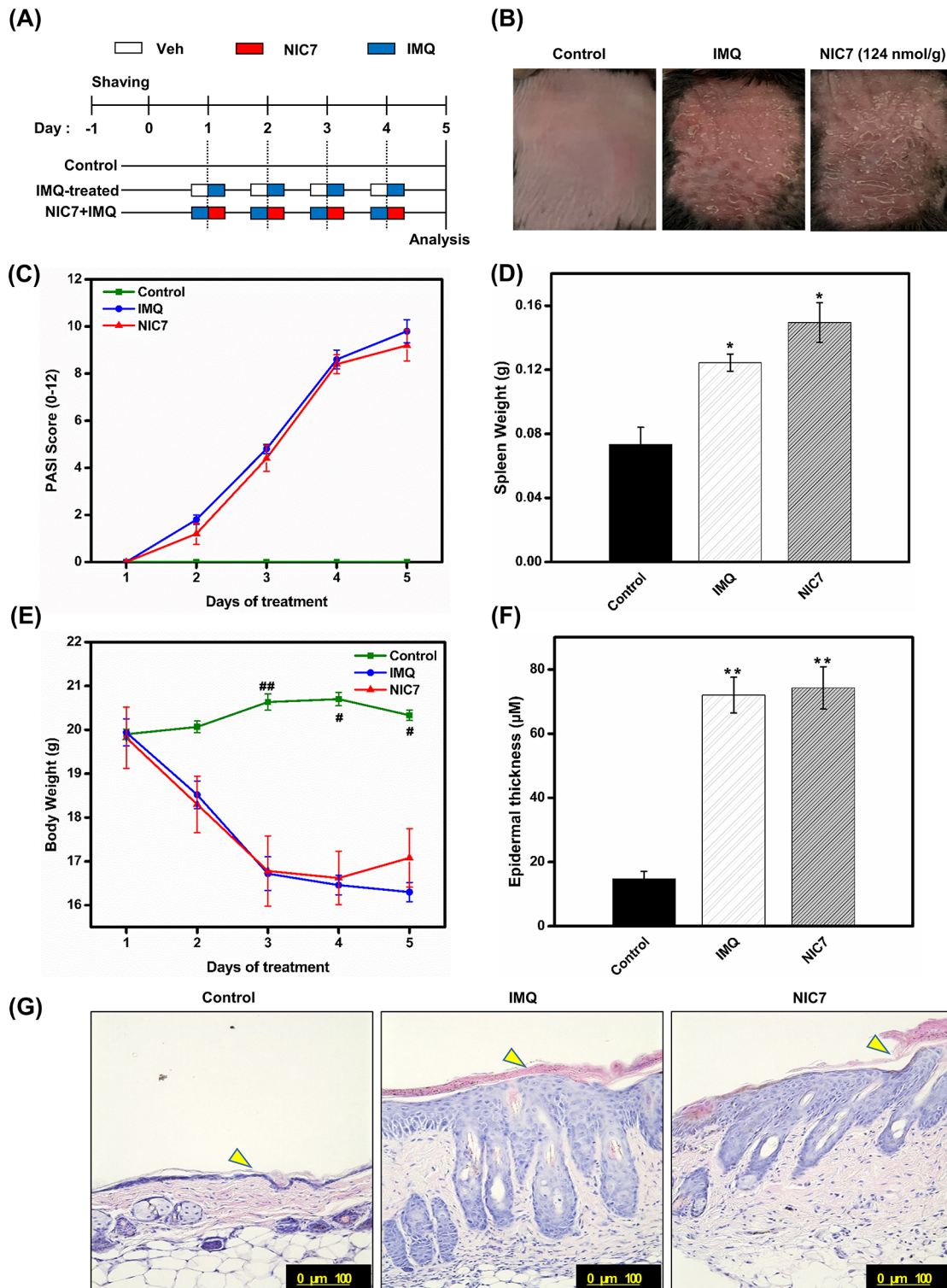


**Figure 5.** Effects of NIC7 in the mouse model of IMQ-induced psoriasis. (A) Summary of the experiment for assessing the therapeutic effect of NIC7 in a mouse model of psoriasis. Psoriasis symptoms were induced by the application of 5% imiquimod (IMQ) cream to the back skin of C57BL/6 mice. The mice were treated daily with 124 nmol/g of NIC7. (B) Shaved back skin of mice on day 4 was examined to monitor the effects of NIC7. (C) Clinical Psoriasis Area and Severity Index (PASI) shows the disease severity score. (D) Effect of NIC7 on spleen weight. (E) Body weight dynamics of the mice during treatment. (F) Epidermis thickness in groups “NIC7” and “IMQ”. (G) Histopathological changes were assessed in the skin by haematoxylin and eosin (H&E) staining to evaluate the thickness of the epidermis (yellow arrow) in the mice with the IMQ-induced psoriasis-like disease. Skin thickness in each group was measured with the Leica DMi8 fluorescence microscope (scale bar: 100  $\mu$ m). Data represent mean  $\pm$  SEM from five skin tissue samples of each group. # $p$  < 0.05 and ## $p$  < 0.01 and \* $p$  < 0.05 and \*\* $p$  < 0.01.

Next, we analyzed the key interactions of NLRP3–NIC7 and NLRP3–NIC7w at 0 ns (initial docked structure) and 50

and 100 ns, respectively (Figure 6E,F). *In silico* molecular docking and simulation suggested that NIC7 and NIC7w

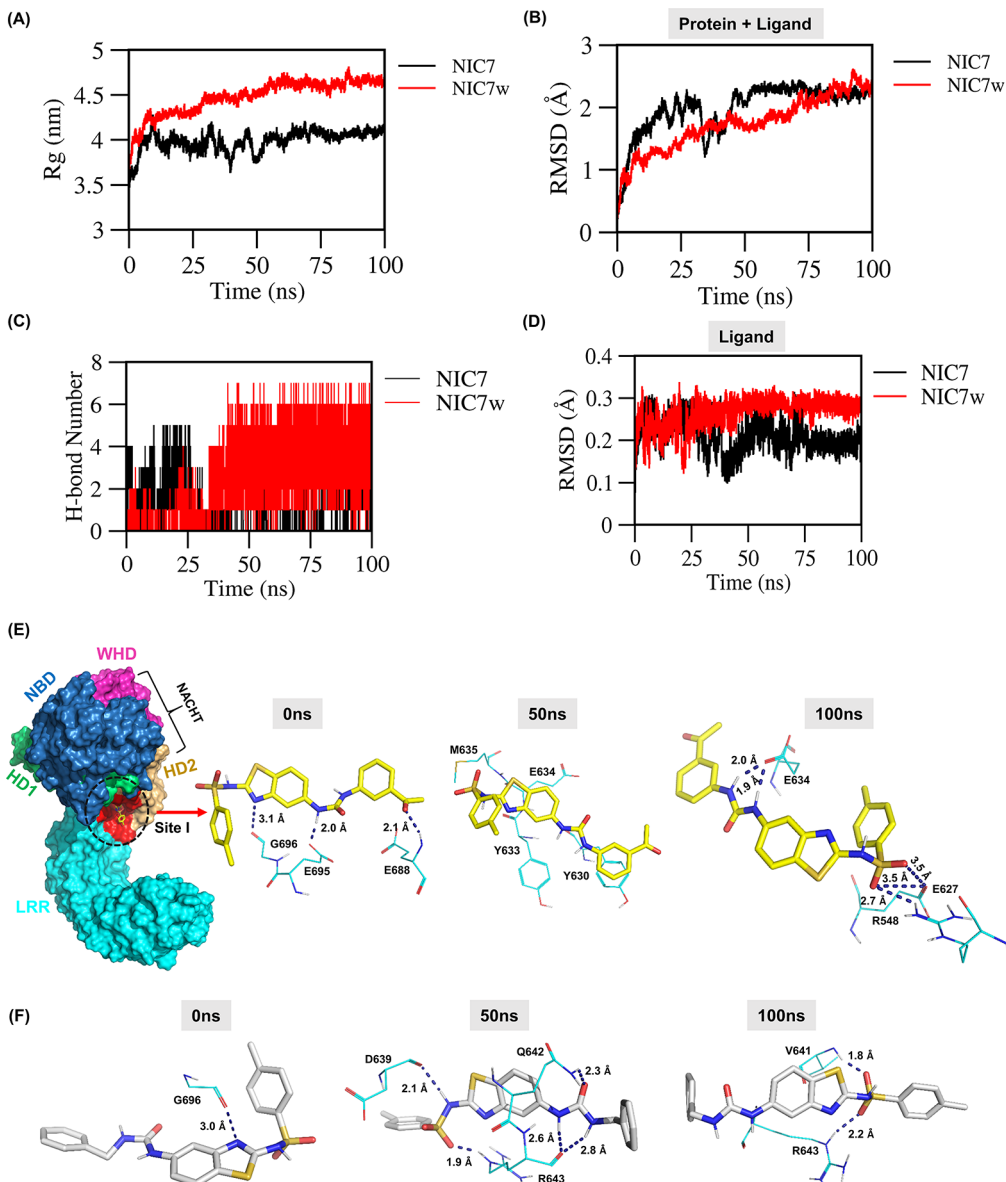


**Figure 6.** Stability and Interaction of NIC7 and NIC7w with NLRP3. (A) Radius of gyration ( $R_g$ ). (B) Root mean square deviation (RMSD) of the NLRP3 bound with NIC7 and NIC7w. (C) Number of hydrogen bonds for both ligands with NLRP3. (D) Root mean square deviation (RMSD) of the ligand NIC7 and NIC7w. (E, F) Interactions of NIC7 and NIC7w occurring within 5 Å of the binding pocket (HD2 domain and LRR domain) of NLRP3 at 0 ns (initial structure) and 50 and 100 ns are shown, respectively. LRR is highlighted in cyan, HD2 in brown, HD1 in green, WHD in purple, and NBD in blue. The pocket is colored in red and the ligand is presented as a stick model. Hydrogen bonds are shown as dashed lines, and the numbers indicate distances in angstroms (Å).

occupy helical domain 2 (HD2) of NLRP3, thus showing similarity of their binding sites. A closer analysis of residues within a distance of 5 Å around our potent ligands revealed that the intermolecular interactions involve similar and distinct amino acid residues of the LRR and HD2 of NLRP3 (Figure 6E). NIC7 at 0 ns contains a mixture of polar and negatively charged residues E688, E695, and G696. The central benzothiazole moiety is stabilized by polar amino acid and form a hydrogen bond with G696 (3.1 Å). The nitrogen atom of the urea group interacts with the side chain of the carboxyl group of E695 (2.0 Å). The acetylphenyl group is buried under the protein's surface, and it forms a hydrogen bond with E688 (2.1 Å). NIC7 does not exhibit bonding at 50 ns, which could be due to a minor fluctuation in the protein. However, it is surrounded by several charged and hydrophobic residues, such

as Y630, Y633, E634, and M635. At 100 ns, it re-establishes the bond and interacts with the charged residues R548, E627, and E634. The nitrogen atoms of urea connect with E634 (1.9 and 2.1 Å), whereas methylbenzenesulfonamide interacts with E627 (3.5 Å) and R548 (2.7 Å) (Figure 6E).

In NIC7w, the initial docked form (at 0 ns) shows interactions of benzothiazole with a nonpolar residue G696 (3.0 Å). At 50 ns, sulfonamide formed bonds with D639 (2.1 Å) and R643 (1.9 Å). Moreover, the urea moiety interacts with the amine of polar Q642 (2.3 Å) and the carboxylic group of charged residue R643 (2.6 and 2.8 Å). The sulfonamide moiety interacts stably with charged residue R643 (2.2 Å) at 50 and 100 ns and also with V641 (1.8 Å) (Figure 6F).

The most effective of all of the derivatives, NIC7w, contains a 1-benzyl group along with a urea group attached to the 3-

benzothiazol-5-yl moiety (Figures 2G and S6), which might provide more stability than NIC7 and have ensured a stronger inhibitory activity against the NLRP3 inflammasome. In addition, several other charged, polar, and nonpolar residues may stabilize the ligands through van der Waals and salt bridge interactions.

**Evaluating Microsomal Stability and CYP Inhibition of NIC7 and NIC7w.** The clearance of a drug by the liver determines its bioavailability and half-life. Liver microsomes are the subcellular fractions that contain drug-metabolizing enzymes. A wide variety of drugs undergo oxidative metabolism by the cytochrome P450 (CYP) enzyme.<sup>56,57</sup> To assess the therapeutic potential of NIC7 and NIC7w, we examined their metabolic stability. The metabolic stability assay revealed the stability of NIC7 and NIC7w up to 19 and 49%, respectively (Table 1). To determine the effect on the

balance and pH,<sup>70</sup> Furthermore, OLT1177 is an active  $\beta$ -sulfonyl nitrile small-molecule drug candidate in clinical phase II for the treatment of osteoarthritis of the knee.<sup>71,72</sup> It has been demonstrated that OLT1177 specifically inhibited the NLRP3 inflammasome and improved the cognitive impairment in the AD mice model.<sup>73</sup> However, no studies have been performed to determine the nitrile group reactivity in OLT1177.<sup>74</sup> Further research is needed to confirm the effect of OLT1177 on other inflammasome activation and clinical therapeutic potential in AD patients.

Nonetheless, the number of specific inhibitors is limited by the unavailability of the crystal structure of NLRP3 bound to a small-molecule modulator. The computational drug discovery is mainly based on the accurate determination of binding site(s) of a ligand on its receptor. There are some alternative approaches such as homology modeling and quantitative structure–activity relationship modeling; however, their accuracy is still questionable.<sup>75</sup> In the present study, we used the cryo-EM structure of human NLRP3 due to the absence of its crystal structure.<sup>41</sup> For structure-based virtual screening, we defined two distinct ligand-binding sites: site I (corresponding to HD2 and LRR of NLRP3 and overlapping with the NEK7-binding site) and site II (corresponding to the NACHT domain of NLRP3). A large multiconformational chemical library was utilized for the *in silico* virtual screening and molecular docking. After close visual evaluation, 19 top-scoring consensus ligands (designated as NIC1–NIC19) were experimentally validated to assess their inhibitory potential on the NLRP3-signaling pathway.

The cell-based screening process led us to shortlist the NIC7 compound based on its better activity to inhibit the NLRP3-mediated release of IL-1 $\beta$  cytokine. To improve the activity, multiple derivatives were developed by modifying the main scaffold of NIC7. The *in vitro* assays confirmed that NIC7w is a better version of NIC7 to inhibit the activation of caspase 1 as well as the release of cytokines and LDH. Of note, both our initial hit (NIC7) and its potent analogue (NIC7w) were docked to the binding pocket of site I. In the cryo-EM structure, the HD2 domain and its surrounding residues have been reported as important binding regions in NLRP3.<sup>41</sup> These findings support the inhibitory efficacy of NIC7 and NIC7w on the NLRP3-mediated signaling pathway.

Adult mammals, including humans, retain the potential of neurogenesis mainly in the subgranular zone of hippocampal dentate gyrus<sup>76,77</sup> and the subventricular zone (SVZ) of lateral ventricles.<sup>78,79</sup> Other controversial neurogenic areas include striatum,<sup>80,81</sup> hypothalamus,<sup>82</sup> amygdala,<sup>83</sup> cortex,<sup>84</sup> and substantia nigra.<sup>85</sup> Certain factors provoke neural stem cells to proliferate during adult neurogenesis.<sup>86,87</sup> The newborn neuronal cells differentiate into lineages such as astrocytes, neurons, and oligodendrocytes.<sup>88,89</sup> Neuroblasts generated in SVZ migrate to the olfactory bulb and differentiate into GABAergic neurons.<sup>90,91</sup> Finally, these neurons establish networking by integrating into the pre-existing circulatory with the help of various neurotransmitters and neurotrophic factors.<sup>92–94</sup> Nonetheless, adult neurogenesis is impaired during the development of AD.<sup>95–98</sup> AD causes neurochemical changes in multiple neurotransmitters and pathological changes in respective receptor systems, including dopaminergic (DAergic),<sup>99</sup> cholinergic,<sup>100</sup> glutamatergic,<sup>101</sup> serotonergic,<sup>102</sup> and adrenergic.<sup>103</sup> Dopamine is a key neurotransmitter involved in synaptic transmission<sup>104</sup> as well as motor cortical plasticity.<sup>105,106</sup> Any damage to the DAergic system deterio-

**Table 1. Microsomal Stability and CYP Inhibition of NIC7 and NIC7w**

	NIC7	NIC7w
microsomal stability (% at 30 min)	human: 19.7%	human: 49.5%
CYP inhibition (% at 10 $\mu$ M)	1A2: <1% 2C9: 34.2% 2C19: <1% 2D6: 9.8% 3A4: <1%	1A2: <1% 2C9: 39.4% 2C19: 15.4% 2D6: 9.1% 3A4: <1%

CYP metabolizing enzyme, NIC7 and NIC7w were treated with various isozymes of CYP (CYP1A2, 2C9, 2C19, 2D6, and 3A4). The information about their associated substrates and used concentrations is shown in Table S3. We observed that NIC7w was able to inhibit 2C9 at 39.4% and 2C19 at 15.4%, suggesting that NIC7w might be capable of producing drug–drug interactions (Table 1). These findings suggest that NIC7 has the most promising properties than NIC7w as a lead for treating AD.

## DISCUSSION

The NLRP3 inflammasome is one of the key components of the innate immune system, which contributes to the development of metabolic and neurodegenerative diseases such as AD, diabetes, and multiple sclerosis.<sup>58–60</sup> The NLRP3 inflammasome activation is triggered by three main signals: mitochondrially generated reactive oxygen species, potassium efflux, and a cathepsin release after lysosomal destabilization.<sup>61</sup> The triggered NLRP3 inflammasome forms a molecular platform to activate caspase 1, which contributes to the maturation of IL-1 $\beta$  and IL-18 as well as induction of pyroptosis.<sup>62</sup> The pharmacological agents are being developed to inhibit the NLRP3 inflammasome signaling pathway, such as MCC950, VX-765, JC-124, parthenolide, BAY 11-7082, harmine, and PLX3397.<sup>39,40,60,63–67</sup> A few of them have shown potent inhibitory activity, suggesting that these compounds might cause the side effects and limit their clinical potential.<sup>68</sup> Parthenolide, BAY 11-7082, and harmine inhibit the NLRP3 inflammasomes, but these drugs are not selective and can inhibit other pathways such as tyrosine kinases, NF- $\kappa$ B, and PPAR.<sup>65–67,69</sup> A potent molecule MCC950 has shown encouraging results in NLRP3-associated disease mice models. Despite this, recent research suggests that MCC950 inhibits the carbonic anhydrase enzyme (CA), which influences carbon dioxide transport in the blood while also maintaining fluid

rates memory and cognitive behavior in AD models,<sup>107–109</sup> and contributes to the early symptoms of AD patients.<sup>110</sup> In AD models, reduction in intraneuronal amyloid deposition and improvement in memory have been observed with the application of dopamine agonists.<sup>111</sup>

In AD patients, gene expression analysis revealed higher expression of NLRP3, ASC, caspase 1, IL-1 $\beta$ , and IL-18.<sup>58</sup> Microglia are reported to be the main cerebral site with NLRP3 components; hence, responsible for the secretion of IL-1 $\beta$  and IL-18.<sup>112,113</sup> Therefore, targeting NLRP3 inflammasome is a subject of active research for the treatment of neurodegenerative diseases such as AD. Here, we evaluated the therapeutic potential of NIC7 in disease models of AD and psoriasis. In AD, NIC7 substantially improved the cognitive behavior of mice along with the recovery of dopamine receptors and regeneration of neuronal markers. Previously, it has been reported that NLRP3 inflammasome contributes to the psoriasis patients with the generation of associated cytokines, i.e., IL-1 $\beta$  and IL-18.<sup>51–53</sup> Hence, we also tested the therapeutic potential of NIC7 in the IMQ-induced disease model of psoriasis. Notably, NIC7 treatment did not improve any symptoms of psoriasis in the IMQ model. This could be because of the development of the psoriasis model with IMQ but not with the recombinant IL-23, which involves the P2X7 receptor-mediated NLRP3-signaling pathway.<sup>55</sup> Psoriasis patients were found to have high levels of TNF- $\alpha$  and IL-6 expression, which was regulated by the NF- $\kappa$ B signaling system.<sup>114</sup> Previous experimental evidence demonstrated that a dual inhibitor BAY 11-7082 of I- $\kappa$ B and NLRP3 reduces the psoriasis symptoms in the IMQ model.<sup>115</sup> Furthermore, NLRP3<sup>-/-</sup> KO mice revealed prolonged NF- $\kappa$ B expression and dermal thickness following IMQ. These findings indicated that NLRP3 is partially involved in the development of psoriasis and might be related to the maintenance of the disease rather than in its onset. Therefore, we hypothesized that the NLRP3-specific inhibitor would be ineffective in an IMQ-induced psoriasis model. In fact, our findings revealed that NIC7 and NIC7w are more NLRP3 specific and do not inhibit TNF- $\alpha$  (Figure S4). Our initial lead, NIC7, and its chemical derivatives contain sulfonamide and urea moieties, which represent important functional groups often found in NLRP3 inflammasome inhibitors and antidiabetic drugs.<sup>39,59</sup> Taken together, these findings indicate that NIC7 may be the most promising lead for treating diseases.

## CONCLUSIONS

Our study suggests that NIC7 is a promising inhibitor of NLRP3-mediated signaling that can successfully alleviate the cognitive impairment observed during AD and, therefore, can act as a lead candidate for the development of NLRP3-specific therapeutics to treat inflammatory diseases and related complications.

## EXPERIMENTAL SECTION

**Cell Lines and Reagents.** THP-1 cells were grown in the RPMI 1640 medium supplemented with 10% of fetal bovine serum (FBS) (Thermo Fisher Scientific, Inc., Waltham, MA) and 1% of a penicillin/streptomycin solution (Gibco). Their differentiation into macrophages was performed by treatment with 80 nM phorbol 12-myristate 13-acetate (PMA) for 24–48 h. The cells were incubated at 5% CO<sub>2</sub> and 37 °C in a humidified incubator (Thermo Fisher Scientific, Inc.). Lipopolysaccharide (LPS; from *Escherichia coli* 0111:

B4) and PMA were purchased from Sigma-Aldrich Co. (St. Louis, MO). Nigericin was acquired from InvivoGen (San Diego, CA).

**Cell Viability Assay.** Cell viability was determined in a colorimetric 1-(4,5-dimethylthiazol-2-yl)-3,5-diphenylformazan (MTT) assay (Sigma-Aldrich Co.). THP-1 (10<sup>5</sup>/well; 24 h) cells were differentiated overnight with PMA (80 nM) in 96-well plates (BD Biosciences, San Jose, CA) and were treated with tested compounds at various concentrations for 24 h. The medium was replaced with a 100 μL/well MTT solution (10%) followed by incubation at 37 °C for 3 h. This solution was replaced with 100 μL/well dimethyl sulfoxide (DMSO), and the plates were further incubated for 30 min at 37 °C. Absorbance in the plate wells was quantitated at a wavelength of 540 nm on a microplate reader (Molecular Devices, Silicon Valley, California). All tested compounds are >95% pure by high-performance liquid chromatography (HPLC).

**Analysis of Cytokines and Lactate Dehydrogenase (LDH).** THP-1 cells (10<sup>5</sup>/well) were differentiated with PMA (80 nM, 48 h) in a 96-well plate (BD Biosciences). The differentiated macrophages were primed with LPS (10 ng/mL) for 4 h. After that, the cells were treated with compounds in the serum-free medium for 1 h, followed by activation of NLRP3 by nigericin for an additional 1 h. The supernatant was collected and analyzed for the secretion levels of human-IL-1 $\beta$  and IL-18 using the respective enzyme-linked immunosorbent assay (ELISA) kits (Thermo Fisher Scientific, Inc.). The supernatant was also analyzed for the release of LDH by means of the LDH Cytotoxicity Detection Kit (Takara, Dalian, China). For the analysis of human-TNF- $\alpha$  and human-IL-8 secretion, the PMA-differentiated THP-1 cells were pretreated with the compounds for 1 h followed by 24 h post-treatment with recombinant human-IL-1 $\beta$  (100 ng/mL). The supernatant was collected and analyzed for the secretion of cytokines with relevant ELISA kits (Thermo Fisher Scientific, Inc.). A microplate spectrophotometer system (Molecular Devices) was employed to read absorbance in the multiwell plate.

**Western Blot Analysis.** For THP-1 cells, NE-PER nuclear and cytoplasmic extraction reagents (Thermo Fisher Scientific, Inc.) containing a protease and phosphatase inhibitor cocktail (Sigma-Aldrich Co.) were used to extract cytoplasmic proteins. The concentration of the total protein was determined with the Bicinchoninic Acid (BCA) Assay Kit (Sigma-Aldrich Co.). The proteins were separated by sodium dodecyl sulfate-polyacrylamide gel electrophoresis (SDS-PAGE) and transferred to a membrane in a Mini-PROTEAN Tetra Cell and Mini Trans-Blot Electrophoretic Transfer Cell System (Bio-Rad Laboratories, Hercules, CA). The membranes were blocked for 1 h with skim milk (5%) and immunoblotted with antibodies against pro-IL-1 $\beta$ , mature IL-1 $\beta$  (Cell Signaling Technology Inc., Danvers, MA), procaspase 1, mature-caspase 1, and  $\beta$ -actin (Santa Cruz Biotechnology Inc., Dallas, TX) at 4 °C overnight. After a wash with phosphate-buffered saline (PBS) supplemented with 0.1% of Tween 20, the membranes were probed with a peroxidase-conjugated anti-rabbit or anti-mouse IgG antibody (1:1000) at room temperature for 2 h. The SuperSignal West Pico ECL solution (Thermo Fisher Scientific, Inc.) was utilized to detect protein bands that were visualized on a ChemiDoc Touch Imaging System (Bio-Rad Laboratories).

**Quantitative Polymerase Chain Reaction (qPCR).** The brain tissues were subdivided into the hippocampus and cortex and crushed with a homogenizer after the addition of PBS. Total RNA was isolated with TRIzol (Ambion, Life Technologies, Carlsbad, CA). The cDNA was synthesized using the Maxime RT preMix (Oligo (dT)15 Primer) Kit (iNtRON Biotechnology, Sungnam, Korea) to perform qPCR with an AccuPower 2X GreenStar qPCR Master Mix (Bioneer, Daejeon, Korea). Expression levels of subtypes of dopamine receptors were analyzed with the primers mentioned in Supporting Table S4. The amount of mRNA was normalized to that of  $\beta$ -actin mRNA. The amplification was carried out using a CFX Connect TM Real-Time PCR System (Bio-Rad), and the data were analyzed using CFX Maestro Software 1.1 (Bio-Rad). The results are presented as the average of three independent experiments.

**Immunohistochemistry.** Cryosections were sectioned into a single layer of cells with the help of a cryotome. The tissue sections

were washed twice with PBS (5 min), treated with 0.1% Triton X-100 and 1% BSA in PBS (15 min), washed two times with PBS (5 min), blocked with 0.5% Tween 20 and 1% BSA in PBS (2 h), washed three times with PBS (5 min), and probed overnight with a primary antibody specific to a nerve regeneration marker, NeuN (ABN78, Millipore, Temecula, CA). The next day, samples were washed three times with PBS (5 min), incubated for 1 h at room temperature with an Alexa 488-conjugated secondary antibody (Invitrogen), washed three times with PBS (5 min), and cover-slipped after staining the nuclei with VECTASHIELD Antifade Mounting Medium with DAPI (H-1200, Vector Laboratories, Burlingame, CA). The staining patterns were measured using a confocal laser-scanning microscope (Fluoview FV 1000, Olympus, Japan).

**Microsomal Stability Assay.** Stock solutions of NIC7 and NIC7w were prepared at a concentration of 10 mM in DMSO and were diluted with 100% methanol to a concentration of 100  $\mu$ M as a working solution. These solutions of NIC7 and NIC7w were diluted with potassium phosphate buffer (10 mM, pH 7.4) to a concentration of 1  $\mu$ M, and then each solution was incubated with 0.5 mg/mL liver microsomes (human) at 37 °C for 5 min. The reaction was initiated by the addition of an NADPH-generating system [3.3 mM glucose-6-phosphate, 1.3 mM  $\beta$ -NADP+, 3.3 mM MgCl<sub>2</sub>, and 0.4 U/mL glucose-6-phosphate dehydrogenase] at 37 °C and 1300 rpm. The reactions were stopped at 0 and 30 min with cold acetonitrile containing carbamazepine as an internal standard at 20 ng/mL. After vortexing and centrifugation, the supernatant was analyzed by liquid chromatography with tandem mass spectrometry (LC-MS/MS). All of the microsomal assays were performed in duplicate.

**Cytochrome P450 Inhibition.** The inhibitory effects of NIC7 and NIC7w on the metabolism of five major P450 probe substrates were evaluated by a previously reported method with minor modifications.<sup>116</sup> A cocktail of substrates (phenacetin O-deethylase, tolbutamide 4-hydroxylase, mephenytoin 4-hydroxylase, dextromethorphan O-demethylase, and midazolam 1'-hydroxylase) was used to test the five major P450 enzymes: 1A2, 2C9, 2C19, 2D6, and 3A4, respectively. NIC7 and NIC7w solutions were prepared at a concentration of 10 mM in DMSO and diluted with methanol to a concentration of 1 mM. The final concentration of the organic solvent (methanol) for cocktail incubation in all of the experiments was set to 1.0% (v/v). The concentrations of all of the substrates in the incubation mixtures are listed in Table S3. Both NIC7 and NIC7w were tested at 10  $\mu$ M, while pooled human liver microsomes were assayed at 0.25 mg/mL. The substrate cocktail solution was incubated with microsomes at 37 °C for 5 min. The reaction was initiated by the addition of the NADPH-generating system (as mentioned above) at 37 °C and 1300 rpm. The reactions were stopped at 10 min by the addition of cold acetonitrile containing carbamazepine as an internal standard at 20 ng/mL. After vortexing and centrifugation, the supernatant was analyzed by LC-MS/MS. All microsomal incubations were performed in triplicate.

**LC-MS/MS Analysis.** After sample preparation, acetonitrile (0.1 mL) containing 20 ng/mL internal standard was added to a 50  $\mu$ L aliquot of each biological sample. After vortexing and centrifugation at 12 000 rpm for 10 min, 10  $\mu$ L of the supernatant was analyzed by LC-MS/MS. In the LC system, a reversed-phase C18 column (BEH C18, 2.1 mm × 100 mm, internal diameter 1.7  $\mu$ m; Waters, Ireland) was kept at 4 °C. The composition of the mobile phase was changed from 80% of 0.1% formic acid in water to 80% of 0.1% formic acid in acetonitrile for 3 min, then switched to 80% of 0.1% formic acid in water for 3.1 min, and maintained for 5 min at 0.5 mL/min. Analytes were monitored on an API5500 triple quadrupole mass spectrometer (AB Sciex, Foster City, CA) equipped with a turbo ion spray interface for electrospray ionization and operated in a positive ion mode at 5.5 kV and 500 °C at an atomizing gas flow of 50 L/min, turbo ion spray gas flow of 50 L/min, curtain gas flow of 20 L/min, ring voltage of 5.5 kV, and collision gas (nitrogen) pressure of 5 Torr. The mass transitions for NIC7, NIC7w, and the internal standard were m/z 481.1 → 165.0 (collision energy 45 eV), 453.1 → 165.0 (41.0 eV), and 236.9 → 194.0 (29 eV), respectively, in multiple-reaction monitoring mode.

**In Vivo Experiments on a Mouse Model of AD.** To determine the therapeutic effects of NIC7 *in vivo*, we used 6-week-old male C57BL/6 mice (19–22 g) and bred them in a feedlot at five mice per cage. To create the AD model, the experimental animals were anesthetized via isoflurane inhalation, followed by an injection of A $\beta$ 1–42 (5  $\mu$ L) using a Hamilton microsyringe with a 26-gauge needle. The Y-maze test and novel object recognition test (for cognitive evaluation) were performed on the AD model mice after training at 20 min/mouse for 2 days before the procedure. The behavioral evaluation was conducted 7 days after the injection of A $\beta$ 1–42. The animals were subdivided into the following groups: AD, NIC7-treated, vehicle (DMSO)-treated, donepezil-treated (positive control), and normal (no disease). The cognitive evaluation was performed on the 7th, 14th, 21st, and 28th day postinjection.

**Behavioral Analysis.** The alteration in spatial cognitive behavior was assessed by means of a Y-maze apparatus with three horizontal identical arms (35 cm long × 15 cm high × 5 cm wide) symmetrically arranged at 120° to each other. Seven days after the A $\beta$  injection, an evaluation was performed in the Y-maze test. After introduction into the Y-maze, each animal was allowed to move freely for 2 min, and then measurement was performed for 5 min. The subject showed a tendency to enter an arm other than that previously visited. The numbers of arm entries and triads were recorded to calculate the percentage of alternations. The entry is defined as the presence of all four limbs within a particular maze arm.

The novel object recognition test was performed in an open-field box containing two identical objects. The mice were first familiarized with these identical objects for 2 min, and later on, one of the objects was replaced with a novel object, and reading was taken for 5 min. The time spent with an identical object (tA) and time spent with a novel object (tB) were calculated, and the recognition index was computed via the formula (tB/(tA + tB)) × 100.

**In Vivo Experiments on a Mouse Model of Psoriasis.** To determine the therapeutic effects of NIC7 *in vivo*, female C57BL/6 mice aged 6–7 weeks were purchased from Orient Bio, Inc. (Seongnam, South Korea). The mice were housed under specific pathogen-free conditions and provided with a standard laboratory diet (ad libitum access to the feed). The psoriasis-related animal experiments were approved by the Institutional Animal Care and Use Committee (IACUC) at Ajou University (Approval No. 2019-0043). Psoriasis-like symptoms were induced by topical application of 62.5 mg of Aldara cream (containing 5% of IMQ; 3 M Pharmaceutical Co., Maplewood, MN) on the shaved back skin of mice for 4 consecutive days. The mice received daily doses of NIC7 (124 nmol/g; i.e., 60 mg/kg) or vehicle as a control by gavage 1 h before the Aldara cream application. After 5 days, the mice were euthanized under respiratory anesthesia, and skin lesions and spleen samples were collected for histological examination. To determine the inflammation severity of the back skin lesions, an objective scoring system was used for daily assessments based on the clinical Psoriasis Area and Severity Index (PASI). Parameters such as erythema, scaling, wrinkling, and thickening were scored independently on a scale from 0 to 4 as follows: 0, none; 1, slight; 2, moderate; 3, marked; and 4, very marked. Erythema, scaling, and thickness were scored under careful observation by experienced researchers. The cumulative score (erythema plus scaling plus thickening, scale 0–12) indicated the severity of psoriasis symptoms.

Skin samples from the back lesions were fixed in a 4% paraformaldehyde solution, embedded in paraffin, sectioned at 4  $\mu$ m thickness, and placed onto glass slides. The sections were then stained with hematoxylin and eosin (H&E) to evaluate the thickness of the dermis and epidermis. Skin thickness was measured under a Leica DMi8 fluorescence microscope by means of a Leica LAS X Hardware Configurator (Leica Microsystems GmbH, Wetzlar, Germany).

**Preparation of a Virtual Screening Library.** Chemical libraries were downloaded from the ZINC database (druglike and leadlike) and from various commercial vendors (Table S1).<sup>117</sup> We subjected the chemical structures to a “wash” procedure using Molecular Operating Environment (MOE) software by considering the removal

of duplicate entries, disconnected groups, salt, and inorganic metal ions.<sup>118</sup> Structures carrying reactive groups were removed, while the largest fragment was kept in the library. Explicit hydrogen atoms were added and re-equilibrated by protonation of strong bases and deprotonation of strong acids at pH 7.0. Intramolecular bonds were scaled to a reasonable length, and up to 10 tautomeric states were listed for each structure (the most feasible tautomer for each ligand). Partial charges for ligands were calculated, and energy minimization was carried out using the Merck molecular force field MMFF94x until a root mean square gradient of 0.01 was reached.

**Analysis of Molecular-Fingerprint-Based Structure Similarity.** Fingerprints were determined for all molecules in the screening library in accordance with the bit-packed MACCS structural keys (FP: BIT MACCS) scheme. In this technique, each molecule is represented by a bit vector that codes for the presence or absence of structural features, where a specific bit position is assigned to each feature. An MOE in-house support vector language script was employed to identify chemical structures with at least 60–75% similarity to the selected NLRP3 antagonist set (Table S2). The search was conducted using a similarity metric (Tanimoto coefficient; TC). TC measures similarity between two (A and B) fingerprints by comparing the common features of each ligand to the total. The similarity metric is based on the following formula: #AB/(#A + #B – #AB), where both A and B are fingerprints, and “#” represents the number of features in each fingerprint. The resulting ligands were stored in a separate library for further screening.

**Preparation of the Protein Structure *In Silico*.** The cryo-electron microscopy (EM) structure of human NLRP3 [Protein Data Bank (PDB) ID: 6NPY] in complex with NEK7 was retrieved from PDB.<sup>41</sup> Unnecessary ligands, including the water present in the structure, were removed. The structure was protonated at pH 7.0, and the energy was minimized by means of the Amber10: the EHT force field until a root mean square gradient of 0.01 was reached.

**Pharmacophore Generation and Screening.** Various pharmacophore models were generated for each ligand on the basis of their best-ranking interactions with either NLRP3 site I or site II. According to the planar-polar-charged-hydrophobic scheme, the pharmacophore features were assigned around important ligand groups. Next, ligand-based virtual screening was performed to identify the structures that conformed to the essential pharmacophore constraints that were applied to each ligand. The resulting hits were combined in a single library and subjected to structure-based virtual screening through molecular docking.

**Structure-Based Virtual Screening.** Virtual screening of the compound library that resulted from the pharmacophore screening was performed on both site I and site II of NLRP3, separately. Site I (Q636, E637, E638, E743, and D748) corresponds to HD2 and LRR of NLRP3, whereas site II (I149, E150, L162, R165, Y166, A225, A226, G227, I228, G229, K230, T231, I232, R235, H258, R260, R349, F371, Y379, P410, L411, W414, F506, V510, I519, and H520) corresponds to the NACHT domain of NLRP3.<sup>41</sup> The docking was conducted by the triangle matcher placement method and London dG scoring function. The ligand poses were rescored using the MMFF94x force field and GBVI/WSA dG scoring function. Residues of NLRP3 were kept rigid, while the ligands remained flexible during the docking calculation. At least 15 different docked poses of each ligand were saved and ranked by their binding-affinity S-score. Each docking round was repeated with the induced-fit docking method, where both the ligand and receptor side chains were allowed to adjust their conformations to obtain the best fit. The top-scoring 19 consensus ligands from both rigid and induced-fit docking rounds were selected for experimental validation of their NLRP3 antagonistic activity.

**Identification of Potent Derivatives of the Initial Lead.** Structural derivatives of the initial lead, NIC7, were retrieved from the MolPort database. For further analysis, only ligands featuring 85–95% structural similarity with the parent scaffold, NIC7, were considered. Approximately 100 ligands were downloaded as SDF files and converted into the PDB format using MOE software. The ligands were washed, and energy was minimized by the same protocol that

was employed to prepare the initial screening library mentioned above. The derivatives were docked and ranked by their binding score toward site I and site II of NLRP3 with the same docking parameters as mentioned in the *Structure-based Virtual Screening* section. The top 25 ligands that fit best in the pocket and showed that maximum interactions were selected for the experimental validation of their antagonistic activity.

**Molecular Dynamics Simulations.** The CHARMM36 all-atom fore field<sup>119</sup> was used to process the docked complexes of NLRP3–NIC7 and NLRP3–NIC7w, which were then solvated inside the 12 Å cubic boxes, followed by the TIP3p water model. The ligand topology was created with the CGenFF server and then converted to a Gromacs-compatible format using a Python script.<sup>120</sup> The simulation systems were neutralized with (Na<sup>+</sup>/Cl<sup>-</sup>), and energy minimization was carried out using the steepest-descent algorithm until a termination gradient of 0.001 KJ mol<sup>-1</sup> was achieved. Then, temperature and pressure equilibration was performed using the Nose–Hoover and Parrinello–Rahman methods, respectively, up to 100 ps.<sup>121</sup> A 1.2 nm distance cut-off was used to quantify short-range electrostatic and van der Waals interactions. The particle mesh Ewald technique was used to determine long-range electrostatic interactions.<sup>122</sup> After equilibration, the GROMACS 2020.4 program<sup>123</sup> was used to run 100 ns molecular dynamics simulations for each system. Data analysis and structural visualization were carried out using the MOE or VMD programs,<sup>124</sup> and GROMACS built-in tools.

**Statistical Analysis.** The presented data are the average of three independent experiments (each experiment was conducted in duplicate), and statistical analysis was performed by two-tailed paired Student's *t*-test. Data were regarded significant at \**P* < 0.05, \*\**P* < 0.01, and \*\*\**P* < 0.001 and #*p* < 0.05, ##*p* < 0.01, and ###*p* < 0.001.

## ASSOCIATED CONTENT

### Supporting Information

The Supporting Information is available free of charge at <https://pubs.acs.org/doi/10.1021/acschemneuro.1c00831>.

Additional figures and tables explaining computational workflow and docking, toxicity and specificity of compounds, the structure of candidates, microsomal stability, cytochrome P450 inhibitions, and primers; an outline of the virtual screening workflow for the identification of primary leads (Figure S1); two sites of NLRP3 were chosen for molecular docking (Figure S2); cell viability measurement (Figure S3); confirming specificity of NIC7 and NIC7w (Figure S4); two-dimensional structures of the first active ligands identified in cell-based assays (Figure S5); two-dimensional structures of active derivatives of NIC7 identified in cell-based assays (Figure S6); chemical compound libraries used for virtual screening (Table S1); the list of NLRP3 inhibitors tested for pharmacophore generation against the multiconformational compound library (Table S2); the CYP enzymes, their substrates, used concentrations, and generated metabolites (Table S3); primer sequences for the expression of dopamine receptors (Table S4) ([PDF](#))

## AUTHOR INFORMATION

### Corresponding Authors

**Wook Kim** — Department of Molecular Science and Technology, Ajou University, Suwon 16499, Korea;  
✉ [orcid.org/0000-0002-7701-4684](https://orcid.org/0000-0002-7701-4684); Email: [wookkim21@ajou.ac.kr](mailto:wookkim21@ajou.ac.kr)  
**Sangdun Choi** — Department of Molecular Science and Technology, Ajou University, Suwon 16499, Korea; S&K Therapeutics, Ajou University Campus Plaza 418,

Yeongtong-gu, Suwon 16502, Korea;  orcid.org/0000-0001-5920-7848; Email: sangdunchoi@ajou.ac.kr

## Authors

- Muhammad Haseeb — Department of Molecular Science and Technology, Ajou University, Suwon 16499, Korea; S&K Therapeutics, Ajou University Campus Plaza 418, Yeongtong-gu, Suwon 16502, Korea;  orcid.org/0000-0003-1224-8276
- Nasir Javaid — Department of Molecular Science and Technology, Ajou University, Suwon 16499, Korea
- Farzana Yasmeen — Department of Molecular Science and Technology, Ajou University, Suwon 16499, Korea
- Uisuk Jeong — Department of Molecular Science and Technology, Ajou University, Suwon 16499, Korea; S&K Therapeutics, Ajou University Campus Plaza 418, Yeongtong-gu, Suwon 16502, Korea
- Ji Hye Han — Department of Molecular Science and Technology, Ajou University, Suwon 16499, Korea
- Juhwan Yoon — Department of Molecular Science and Technology, Ajou University, Suwon 16499, Korea
- Jee Yeon Seo — Whan In Pharmaceutical Co., Ltd., Songpa-gu, Seoul 05855, Korea
- Jae Kyung Heo — Whan In Pharmaceutical Co., Ltd., Songpa-gu, Seoul 05855, Korea
- Ho Chul Shin — Whan In Pharmaceutical Co., Ltd., Songpa-gu, Seoul 05855, Korea
- Moon Suk Kim — Department of Molecular Science and Technology, Ajou University, Suwon 16499, Korea;  orcid.org/0000-0002-6689-1825

Complete contact information is available at:  
<https://pubs.acs.org/10.1021/acschemneuro.1c00831>

## Author Contributions

¶M.H. and N.J. contributed equally to the work. M.H.: conceptualization, methodology, investigation, data curation, formal analysis, and writing—original draft. N.J.: methodology, investigation, data curation, formal analysis, and writing—original draft. F.Y.: methodology and investigation. U.J.: investigation. J.H.H.: investigation. J.Y.: investigation. J.Y.S.: data curation and formal analysis. J.K.H.: data curation and formal analysis. H.C.S.: funding acquisition. M.S.K.: funding acquisition. W.K.: data curation and formal analysis, writing—original draft. S.C.: conceptualization, methodology, data curation, formal analysis, and writing—original draft, and funding acquisition.

## Funding

This study was funded by the Korea Drug Development Fund, which is administered by the Ministry of Science and ICT, the Ministry of Trade, Industry, and Energy, and the Ministry of Health and Welfare (HN21C1058, Republic of Korea). The National Research Foundation of Korea [2022M3A9G1014520, 2019M3D1A1078940, and 2019R1A6A1A11051471] also provided funding for this research. The sponsor had no role in study design; in the collection, analysis, and interpretation of the data; in the writing of the report; and in the decision to submit the article for publication.

## Notes

The authors declare no competing financial interest.

## ■ ABBREVIATIONS

NLRP3, nucleotide-binding oligomerization domain (NOD)-like receptor family pyrin domain-containing 3; AD, Alzheimer's disease; NIC7, NLRP3-inhibitory compound 7; IL-1 $\beta$ , interleukin-1  $\beta$ ; IL-18, interleukin-18; LPS, lipopolysaccharide; IMQ, imiquimod; PMA, phorbol 12-myristate 13-acetate; IC<sub>50</sub>, half-maximal inhibitory concentrations; LDH, lactate dehydrogenase; TNF- $\alpha$ , tumor necrosis factor-alpha; PASI, psoriasis area and severity index; HD2, helical domain 2; LRR, leucine-rich repeat; CYP, cytochrome P450; H&E, hematoxylin and eosin; A $\beta$  1–42, amyloid  $\beta$  protein 1–42

## ■ REFERENCES

- (1) de Zoete, M. R.; Palm, N. W.; Zhu, S.; Flavell, R. A. Inflammasomes. *Cold Spring Harbor Perspect. Biol.* **2014**, *6*, No. a016287.
- (2) Guo, H.; Callaway, J. B.; Ting, J. P. Inflammasomes: mechanism of action, role in disease, and therapeutics. *Nat. Med.* **2015**, *21*, 677–687.
- (3) Wen, H.; Miao, E. A.; Ting, J. P. Mechanisms of NOD-like receptor-associated inflammasome activation. *Immunity* **2013**, *39*, 432–441.
- (4) Lamkanfi, M.; Dixit, V. M. Mechanisms and functions of inflammasomes. *Cell* **2014**, *157*, 1013–1022.
- (5) de Rivero Vaccari, J. P.; Dietrich, W. D.; Keane, R. W. Activation and regulation of cellular inflammasomes: gaps in our knowledge for central nervous system injury. *J. Cereb. Blood Flow Metab.* **2014**, *34*, 369–375.
- (6) Zhou, K.; Shi, L.; Wang, Y.; Chen, S.; Zhang, J. Recent Advances of the NLRP3 Inflammasome in Central Nervous System Disorders. *J. Immunol. Res.* **2016**, *2016*, 1–9.
- (7) Schroder, K.; Tschoop, J. The inflammasomes. *Cell* **2010**, *140*, 821–832.
- (8) Sagulenko, V.; Thygesen, S. J.; Sester, D. P.; Idris, A.; Cridland, J. A.; Vajjhala, P. R.; Roberts, T. L.; Schroder, K.; Vince, J. E.; Hill, J. M.; Silke, J.; Stacey, K. J. AIM2 and NLRP3 inflammasomes activate both apoptotic and pyroptotic death pathways via ASC. *Cell Death Differ.* **2013**, *20*, 1149–1160.
- (9) Shi, J.; Zhao, Y.; Wang, Y.; Gao, W.; Ding, J.; Li, P.; Hu, L.; Shao, F. Inflammatory caspases are innate immune receptors for intracellular LPS. *Nature* **2014**, *514*, 187–192.
- (10) He, Y.; Zeng, M. Y.; Yang, D.; Motro, B.; Nunez, G. NEK7 is an essential mediator of NLRP3 activation downstream of potassium efflux. *Nature* **2016**, *530*, 354–357.
- (11) Strowig, T.; Henao-Mejia, J.; Elinav, E.; Flavell, R. Inflammasomes in health and disease. *Nature* **2012**, *481*, 278–286.
- (12) Wen, H.; Ting, J. P.; O'Neill, L. A. A role for the NLRP3 inflammasome in metabolic diseases—did Warburg miss inflammation? *Nat. Immunol.* **2012**, *13*, 352–357.
- (13) Heneka, M. T.; Kummer, M. P.; Stutz, A.; Delekate, A.; Schwartz, S.; Vieira-Saecker, A.; Griep, A.; Axt, D.; Remus, A.; Tzeng, T. C.; Gelpi, E.; Halle, A.; Korte, M.; Latz, E.; Golenbock, D. T. NLRP3 is activated in Alzheimer's disease and contributes to pathology in APP/PS1 mice. *Nature* **2013**, *493*, 674–678.
- (14) Scearce-Levie, K. Monitoring spatial learning and memory in Alzheimer's disease mouse models using the Morris Water Maze. In *Alzheimer's Disease and Frontotemporal Dementia*; Springer, 2010; pp 191–205.
- (15) Edwards, S. R.; Hamlin, A. S.; Marks, N.; Coulson, E. J.; Smith, M. T. Comparative studies using the Morris water maze to assess spatial memory deficits in two transgenic mouse models of Alzheimer's disease. *Clin. Exp. Pharmacol. Physiol.* **2014**, *41*, 798–806.
- (16) Ubundit, N.; Wattanathorn, J.; Mucimapura, S.; Ingkaninan, K. Cognitive enhancement and neuroprotective effects of Bacopa monnieri in Alzheimer's disease model. *J. Ethnopharmacol.* **2010**, *127*, 26–31.

- (17) Wang, Y.; Liu, J.; Zhang, Z.; Bi, P.; Qi, Z.; Zhang, C. Anti-neuroinflammation effect of ginsenoside Rbl in a rat model of Alzheimer disease. *Neurosci. Lett.* **2011**, *487*, 70–72.
- (18) Bromley-Brits, K.; Deng, Y.; Song, W. Morris water maze test for learning and memory deficits in Alzheimer's disease model mice. *J. Visualized Exp.* **2011**, No. e2920.
- (19) D'Hooge, R.; De Deyn, P. P. Applications of the Morris water maze in the study of learning and memory. *Brain Res. Rev.* **2001**, *36*, 60–90.
- (20) Kraeuter, A.-K.; Guest, P. C.; Sarnyai, Z. The Y-maze for assessment of spatial working and reference memory in mice. In *Pre-Clinical Models*; Springer, 2019; pp 105–111.
- (21) Prieur, E. A.; Jadavji, N. M. Assessing spatial working memory using the spontaneous alternation Y-maze test in aged male mice. *Bio-Protoc.* **2019**, *9*, No. e3162.
- (22) Stewart, S.; Cacucci, F.; Lever, C. Which memory task for my mouse? A systematic review of spatial memory performance in the Tg2576 Alzheimer's mouse model. *J. Alzheimer's Dis.* **2011**, *26*, 105–126.
- (23) King, D. L.; Arendash, G. W. Behavioral characterization of the Tg2576 transgenic model of Alzheimer's disease through 19 months. *Physiol. Behav.* **2002**, *75*, 627–642.
- (24) Zhang, R.; Xue, G.; Wang, S.; Zhang, L.; Shi, C.; Xie, X. Novel object recognition as a facile behavior test for evaluating drug effects in A $\beta$ PP/PS1 Alzheimer's disease mouse model. *J. Alzheimer's Dis.* **2012**, *31*, 801–812.
- (25) Dodart, J. C.; Mathis, C.; Ungerer, A. Scopolamine-induced deficits in a two-trial object recognition task in mice. *NeuroReport* **1997**, *8*, 1173–1178.
- (26) Alkam, T.; Nitta, A.; Mizoguchi, H.; Itoh, A.; Nabeshima, T. A natural scavenger of peroxy nitrites, rosmarinic acid, protects against impairment of memory induced by A $\beta$ 25–35. *Behav. Brain Res.* **2007**, *180*, 139–145.
- (27) Greco, S. J.; Bryan, K. J.; Sarkar, S.; Zhu, X.; Smith, M. A.; Ashford, J. W.; Johnston, J. M.; Tezapsidis, N.; Casadesus, G. Leptin reduces pathology and improves memory in a transgenic mouse model of Alzheimer's disease. *J. Alzheimer's Dis.* **2010**, *19*, 1155–1167.
- (28) Yuede, C. M.; Zimmerman, S. D.; Dong, H.; Kling, M. J.; Bero, A. W.; Holtzman, D. M.; Timson, B. F.; Csernansky, J. G. Effects of voluntary and forced exercise on plaque deposition, hippocampal volume, and behavior in the Tg2576 mouse model of Alzheimer's disease. *Neurobiol. Dis.* **2009**, *35*, 426–432.
- (29) Jardanhazi-Kurutz, D.; Kummer, M. P.; Terwel, D.; Vogel, K.; Dyrks, T.; Thiele, A.; Heneka, M. T. Induced LC degeneration in APP/PS1 transgenic mice accelerates early cerebral amyloidosis and cognitive deficits. *Neurochem. Int.* **2010**, *57*, 375–382.
- (30) Wang, W.; Zhou, Q.; Jiang, T.; Li, S.; Ye, J.; Zheng, J.; Wang, X.; Liu, Y.; Deng, M.; Ke, D.; et al. A novel small-molecule PROTAC selectively promotes tau clearance to improve cognitive functions in Alzheimer-like models. *Theranostics* **2021**, *11*, 5279.
- (31) D'agostino, G.; Russo, R.; Avagliano, C.; Cristiano, C.; Meli, R.; Calignano, A. Palmitoylethanolamide protects against the amyloid- $\beta$  25–35-induced learning and memory impairment in mice, an experimental model of Alzheimer disease. *Neuropsychopharmacology* **2012**, *37*, 1784–1792.
- (32) Dinarello, C. A.; Novick, D.; Kim, S.; Kaplanski, G. Interleukin-18 and IL-18 binding protein. *Front. Immunol.* **2013**, *4*, 289.
- (33) Jesus, A. A.; Goldbach-Mansky, R. IL-1 blockade in autoinflammatory syndromes. *Annu. Rev. Med.* **2014**, *65*, 223–244.
- (34) Lamkanfi, M.; Mueller, J. L.; Vitari, A. C.; Misagh, S.; Fedorova, A.; Deshayes, K.; Lee, W. P.; Hoffman, H. M.; Dixit, V. M. Glyburide inhibits the Cryopyrin/Nalp3 inflammasome. *J. Cell Biol.* **2009**, *187*, 61–70.
- (35) Juliana, C.; Fernandes-Alnemri, T.; Wu, J.; Datta, P.; Solorzano, L.; Yu, J. W.; Meng, R.; Quong, A. A.; Latz, E.; Scott, C. P.; Alnemri, E. S. Anti-inflammatory compounds parthenolide and Bay 11-7082 are direct inhibitors of the inflammasome. *J. Biol. Chem.* **2010**, *285*, 9792–9802.
- (36) Coll, R. C.; O'Neill, L. A. J. The cytokine release inhibitory drug CRID3 targets ASC oligomerisation in the NLRP3 and AIM2 inflammasomes. *PLoS One* **2011**, *6*, No. e29539.
- (37) Isakov, E.; Weisman-Shomer, P.; Benhar, M. Suppression of the pro-inflammatory NLRP3/interleukin-1beta pathway in macrophages by the thioredoxin reductase inhibitor auranofin. *Biochim. Biophys. Acta, Gen. Subj.* **2014**, *1840*, 3153–3161.
- (38) Youm, Y. H.; Nguyen, K. Y.; Grant, R. W.; Goldberg, E. L.; Bodogai, M.; Kim, D.; D'Agostino, D.; Planavsky, N.; Lupfer, C.; Kanneganti, T. D.; Kang, S.; Horvath, T. L.; Fahmy, T. M.; Crawford, P. A.; Biragyn, A.; Alnemri, E.; Dixit, V. D. The ketone metabolite beta-hydroxybutyrate blocks NLRP3 inflammasome-mediated inflammatory disease. *Nat. Med.* **2015**, *21*, 263–269.
- (39) Coll, R. C.; Robertson, A. A.; Chae, J. J.; Higgins, S. C.; Munoz-Planillo, R.; Inserra, M. C.; Vetter, I.; Dungan, L. S.; Monks, B. G.; Stutz, A.; Croker, D. E.; Butler, M. S.; Haneklaus, M.; Sutton, C. E.; Nunez, G.; Latz, E.; Kastner, D. L.; Mills, K. H.; Masters, S. L.; Schroder, K.; Cooper, M. A.; O'Neill, L. A. A small-molecule inhibitor of the NLRP3 inflammasome for the treatment of inflammatory diseases. *Nat. Med.* **2015**, *21*, 248–255.
- (40) Yin, J.; Zhao, F.; Chojnacki, J. E.; Fulp, J.; Klein, W. L.; Zhang, S.; Zhu, X. NLRP3 Inflammasome Inhibitor Ameliorates Amyloid Pathology in a Mouse Model of Alzheimer's Disease. *Mol. Neurobiol.* **2018**, *55*, 1977–1987.
- (41) Sharif, H.; Wang, L.; Wang, W. L.; Magupalli, V. G.; Andreeva, L.; Qiao, Q.; Hauenstein, A. V.; Wu, Z.; Nunez, G.; Mao, Y.; Wu, H. Structural mechanism for NEK7-licensed activation of NLRP3 inflammasome. *Nature* **2019**, *570*, 338–343.
- (42) Broadbent, N. J.; Squire, L. R.; Clark, R. E. Spatial memory, recognition memory, and the hippocampus. *Proc. Natl. Acad. Sci. U.S.A.* **2004**, *101*, 14515–14520.
- (43) Storga, D.; Vrecko, K.; Birkmayer, J. G.; Reibnegger, G. Monoaminergic neurotransmitters, their precursors and metabolites in brains of Alzheimer patients. *Neurosci. Lett.* **1996**, *203*, 29–32.
- (44) Reinikainen, K. J.; Soininen, H.; Riekkinen, P. J. Neurotransmitter changes in Alzheimer's disease: implications to diagnostics and therapy. *J. Neurosci. Res.* **1990**, *27*, 576–586.
- (45) Pan, X.; Kaminga, A. C.; Wen, S. W.; Wu, X.; Acheampong, K.; Liu, A. Dopamine and dopamine receptors in Alzheimer's disease: a systematic review and network meta-analysis. *Front. Aging Neurosci.* **2019**, *11*, 175.
- (46) Deby, B.; Schmülling, L.; Zhou, L.; Rune, G.; Beyer, C.; Johann, S. Neurodegeneration and NLRP3 inflammasome expression in the anterior thalamus of SOD1 (G93A) ALS mice. *Brain Pathol.* **2018**, *28*, 14–27.
- (47) de Rivero Vaccari, J. P.; Lotocki, G.; Marcillo, A. E.; Dietrich, W. D.; Keane, R. W. A molecular platform in neurons regulates inflammation after spinal cord injury. *J. Neurosci.* **2008**, *28*, 3404–3414.
- (48) Yang-Wei Fann, D.; Lee, S.; Manzanero, S.; Tang, S.-C.; Gelderblom, M.; Chunduri, P.; Bernreuther, C.; Glatzel, M.; Cheng, Y.-L.; Thundyil, J. Intravenous immunoglobulin suppresses NLRP1 and NLRP3 inflammasome-mediated neuronal death in ischemic stroke. *Cell Death Dis.* **2013**, *4*, e790.
- (49) Zendedel, A.; Johann, S.; Mehrabi, S.; Joghataei, M.-t.; Hassanzadeh, G.; Kipp, M.; Beyer, C. Activation and regulation of NLRP3 inflammasome by intrathecal application of SDF-1 $\alpha$  in a spinal cord injury model. *Mol. Neurobiol.* **2016**, *53*, 3063–3075.
- (50) Schon, M. P.; Boehncke, W. H.; Brocker, E. B. Psoriasis: Clinical manifestations, pathogenesis and therapeutic perspectives. *Discovery Med.* **2005**, *5*, 253–258.
- (51) Carlström, M.; Ekman, A. K.; Petersson, S.; Soderkvist, P.; Enerback, C. Genetic support for the role of the NLRP3 inflammasome in psoriasis susceptibility. *Exp. Dermatol.* **2012**, *21*, 932–937.
- (52) Rabeony, H.; Pohin, M.; Vasseur, P.; Petit-Paris, I.; Jegou, J. F.; Favot, L.; Frouin, E.; Boutet, M. A.; Blanchard, F.; Togbe, D.; Ryffel, B.; Bernard, F. X.; Lecron, J. C.; Morel, F. IMQ-induced skin inflammation in mice is dependent on IL-1R1 and MyD88 signaling

- but independent of the NLRP3 inflammasome. *Eur. J. Immunol.* **2015**, *45*, 2847–2857.
- (53) Verma, D.; Fekri, S. Z.; Sigurdardottir, G.; Bivik Eding, C.; Sandin, C.; Enerback, C. Enhanced Inflammasome Activity in Patients with Psoriasis Promotes Systemic Inflammation. *J. Invest. Dermatol.* **2021**, *141*, 586–595 e585.
- (54) Walter, A.; Schafer, M.; Cecconi, V.; Matter, C.; Urosevic-Maiwald, M.; Belloni, B.; Schonewolf, N.; Dummer, R.; Bloch, W.; Werner, S.; Beer, H. D.; Knuth, A.; van den Broek, M. Aldara activates TLR7-independent immune defence. *Nat. Commun.* **2013**, *4*, No. 1560.
- (55) Diaz-Perez, J. A.; Killeen, M. E.; Yang, Y.; Carey, C. D.; Falo, L. D., Jr.; Mathers, A. R. Extracellular ATP and IL-23 Form a Local Inflammatory Circuit Leading to the Development of a Neutrophil-Dependent Psoriasiform Dermatitis. *J. Invest. Dermatol.* **2018**, *138*, 2595–2605.
- (56) Obach, R. S. Prediction of human clearance of twenty-nine drugs from hepatic microsomal intrinsic clearance data: an examination of in vitro half-life approach and nonspecific binding to microsomes. *Drug Metab. Dispos.* **1999**, *27*, 1350–1359.
- (57) Guengerich, F. P. Role of cytochrome P450 enzymes in drug-drug interactions. *Adv. Pharmacol.* **1997**, *43*, 7–35.
- (58) Saresella, M.; La Rosa, F.; Piancone, F.; Zoppis, M.; Marventano, I.; Calabrese, E.; Rainone, V.; Nemni, R.; Mancuso, R.; Clerici, M. The NLRP3 and NLRP1 inflammasomes are activated in Alzheimer's disease. *Mol. Neurodegener.* **2016**, *11*, No. 23.
- (59) Seino, S. Cell signalling in insulin secretion: the molecular targets of ATP, cAMP and sulfonylurea. *Diabetologia* **2012**, *55*, 2096–2108.
- (60) McKenzie, B. A.; Mamik, M. K.; Saito, L. B.; Boghozian, R.; Monaco, M. C.; Major, E. O.; Lu, J. Q.; Branton, W. G.; Power, C. Caspase-1 inhibition prevents glial inflammasome activation and pyroptosis in models of multiple sclerosis. *Proc. Natl. Acad. Sci. U.S.A.* **2018**, *115*, E6065–E6074.
- (61) Gao, L.; Dong, Q.; Song, Z.; Shen, F.; Shi, J.; Li, Y. NLRP3 inflammasome: a promising target in ischemic stroke. *Inflammation Res.* **2017**, *66*, 17–24.
- (62) Liu, H. D.; Li, W.; Chen, Z. R.; Hu, Y. C.; Zhang, D. D.; Shen, W.; Zhou, M. L.; Zhu, L.; Hang, C. H. Expression of the NLRP3 inflammasome in cerebral cortex after traumatic brain injury in a rat model. *Neurochem. Res.* **2013**, *38*, 2072–2083.
- (63) Flores, J.; Noel, A.; Foveau, B.; Lynham, J.; LeCrux, C.; LeBlanc, A. C. Caspase-1 inhibition alleviates cognitive impairment and neuropathology in an Alzheimer's disease mouse model. *Nat. Commun.* **2018**, *9*, No. 3916.
- (64) Jin, W. N.; Shi, S. X.; Li, Z.; Li, M.; Wood, K.; Gonzales, R. J.; Liu, Q. Depletion of microglia exacerbates postischemic inflammation and brain injury. *J. Cereb. Blood Flow Metab.* **2017**, *37*, 2224–2236.
- (65) Yip, K. H.; Zheng, M. H.; Feng, H. T.; Steer, J. H.; Joyce, D. A.; Xu, J. Sesquiterpene lactone parthenolide blocks lipopolysaccharide-induced osteolysis through the suppression of NF- $\kappa$ B activity. *J. Bone Miner. Res.* **2004**, *19*, 1905–1916.
- (66) Strickson, S.; Campbell, D. G.; Emmerich, C. H.; Knebel, A.; Plater, L.; Ritoro, M. S.; Shapiro, N.; Cohen, P. The anti-inflammatory drug BAY 11-7082 suppresses the MyD88-dependent signalling network by targeting the ubiquitin system. *Biochem. J.* **2013**, *451*, 427–437.
- (67) Waki, H.; Park, K. W.; Mitro, N.; Pei, L.; Damoiseaux, R.; Wilpitz, D. C.; Reue, K.; Saez, E.; Tontonoz, P. The small molecule harmine is an antidiabetic cell-type-specific regulator of PPARgamma expression. *Cell Metab.* **2007**, *5*, 357–370.
- (68) Jiang, H.; He, H.; Chen, Y.; Huang, W.; Cheng, J.; Ye, J.; Wang, A.; Tao, J.; Wang, C.; Liu, Q.; Jin, T.; Jiang, W.; Deng, X.; Zhou, R. Identification of a selective and direct NLRP3 inhibitor to treat inflammatory disorders. *J. Exp. Med.* **2017**, *214*, 3219–3238.
- (69) Wang, W. Y.; Wu, Y. C.; Wu, C. C. Prevention of platelet glycoprotein IIb/IIIa activation by 3,4-methylenedioxyl-beta-nitrostyrene, a novel tyrosine kinase inhibitor. *Mol. Pharmacol.* **2006**, *70*, 1380–1389.
- (70) Kennedy, C. R.; Goya Grocic, A.; Kovacic, T.; Singh, R.; Ward, J. A.; Shenoy, A. R.; Tate, E. W. A Probe for NLRP3 Inflammasome Inhibitor MCC950 Identifies Carbonic Anhydrase 2 as a Novel Target. *ACS Chem. Biol.* **2021**, *16*, 982–990.
- (71) [www.clinicaltrials.gov](https://www.clinicaltrials.gov) Trials n. NCT02134964, N., NCT02104050, NCT03534297, EudraCT 2016-000943-14.
- (72) Marchetti, C.; Swartzwelder, B.; Gamboni, F.; Neff, C. P.; Richter, K.; Azam, T.; Carta, S.; Tengesdal, I.; Nemkov, T.; D'Alessandro, A.; Henry, C.; Jones, G. S.; Goodrich, S. A.; St Laurent, J. P.; Jones, T. M.; Scribner, C. L.; Barrow, R. B.; Altman, R. D.; Skouras, D. B.; Gattorno, M.; Grau, V.; Janciauskienė, S.; Rubartelli, A.; Joosten, L. A. B.; Dinarello, C. A. OLT1177, a betasulfonyl nitrile compound, safe in humans, inhibits the NLRP3 inflammasome and reverses the metabolic cost of inflammation. *Proc. Natl. Acad. Sci. U.S.A.* **2018**, *115*, E1530–E1539.
- (73) Lonnemann, N.; Hosseini, S.; Marchetti, C.; Skouras, D. B.; Stefanoni, D.; D'Alessandro, A.; Dinarello, C. A.; Korte, M. The NLRP3 inflammasome inhibitor OLT1177 rescues cognitive impairment in a mouse model of Alzheimer's disease. *Proc. Natl. Acad. Sci. U.S.A.* **2020**, *117*, 32145–32154.
- (74) Bertinaria, M.; Gastaldi, S.; Marini, E.; Giorgis, M. Development of covalent NLRP3 inflammasome inhibitors: Chemistry and biological activity. *Arch. Biochem. Biophys.* **2019**, *670*, 116–139.
- (75) Sliwoski, G.; Kothiwale, S.; Meiler, J.; Lowe, E. W., Jr. Computational methods in drug discovery. *Pharmacol. Rev.* **2014**, *66*, 334–395.
- (76) Bonaguidi, M. A.; Song, J.; Ming, G.-I.; Song, H. A unifying hypothesis on mammalian neural stem cell properties in the adult hippocampus. *Curr. Opin. Neurobiol.* **2012**, *22*, 754–761.
- (77) Kempermann, G.; Song, H.; Gage, F. H. Neurogenesis in the adult hippocampus. *Cold Spring Harbor Perspect. Biol.* **2015**, *7*, No. a018812.
- (78) Ponti, G.; Obernier, K.; Alvarez-Buylla, A. *Lineage Progression from Stem Cells to New Neurons in the Adult Brain Ventricular-Subventricular Zone*; Taylor & Francis, 2013; pp 1649–1650.
- (79) García-Verdugo, J. M.; Doetsch, F.; Wichterle, H.; Lim, D. A.; Alvarez-Buylla, A. Architecture and cell types of the adult subventricular zone: in search of the stem cells. *J. Neurobiol.* **1998**, *36*, 234–248.
- (80) Shapiro, L. A.; Ng, K.; Zhou, Q.-Y.; Ribak, C. E. Subventricular zone-derived, newly generated neurons populate several olfactory and limbic forebrain regions. *Epilepsy Behav.* **2009**, *14*, 74–80.
- (81) Suzuki, S. O.; Goldman, J. E. Multiple cell populations in the early postnatal subventricular zone take distinct migratory pathways: a dynamic study of glial and neuronal progenitor migration. *J. Neurosci.* **2003**, *23*, 4240–4250.
- (82) Evans, J.; Summers, C.; Moore, J.; Huentelman, M. J.; Deng, J.; Gelband, C. H.; Shaw, G. Characterization of mitotic neurons derived from adult rat hypothalamus and brain stem. *J. Neurophysiol.* **2002**, *87*, 1076–1085.
- (83) Bernier, P. J.; Bédard, A.; Vinet, J.; Lévesque, M.; Parent, A. Newly generated neurons in the amygdala and adjoining cortex of adult primates. *Proc. Natl. Acad. Sci. U.S.A.* **2002**, *99*, 11464–11469.
- (84) Magavi, S. S.; Leavitt, B. R.; Macklis, J. D. Induction of neurogenesis in the neocortex of adult mice. *Nature* **2000**, *405*, 951–955.
- (85) Zhao, M.; Momma, S.; Delfani, K.; Carlén, M.; Cassidy, R. M.; Johansson, C. B.; Brismar, H.; Shupliakov, O.; Frisén, J.; Janson, A. M. Evidence for neurogenesis in the adult mammalian substantia nigra. *Proc. Natl. Acad. Sci. U.S.A.* **2003**, *100*, 7925–7930.
- (86) Lie, D.-C.; Colamarino, S. A.; Song, H.-J.; Désiré, L.; Mira, H.; Consiglio, A.; Lein, E. S.; Jessberger, S.; Lansford, H.; Dearie, A. R.; Gage, F. H. Wnt signalling regulates adult hippocampal neurogenesis. *Nature* **2005**, *437*, 1370–1375.
- (87) Lai, K.; Kaspar, B. K.; Gage, F. H.; Schaffer, D. V. Sonic hedgehog regulates adult neural progenitor proliferation in vitro and in vivo. *Nat. Neurosci.* **2003**, *6*, 21–27.
- (88) Gage, F. H. Mammalian neural stem cells. *Science* **2000**, *287*, 1433–1438.

- (89) Jessberger, S.; Toni, N.; Clemenson, G. D., Jr; Ray, J.; Gage, F. H. Directed differentiation of hippocampal stem/progenitor cells in the adult brain. *Nat. Neurosci.* **2008**, *11*, 888–893.
- (90) Lois, C.; Garcia-Verdugo, J.-M.; Alvarez-Buylla, A. Chain migration of neuronal precursors. *Science* **1996**, *271*, 978–981.
- (91) Magavi, S. S. P.; Mitchell, B. D.; Szentirmai, O.; Carter, B. S.; Macklis, J. D. Adult-born and preexisting olfactory granule neurons undergo distinct experience-dependent modifications of their olfactory responses in vivo. *J. Neurosci.* **2005**, *25*, 10729–10739.
- (92) Nissant, A.; Bardy, C.; Katagiri, H.; Murray, K.; Lledo, P.-M. Adult neurogenesis promotes synaptic plasticity in the olfactory bulb. *Nat. Neurosci.* **2009**, *12*, 728–730.
- (93) Carleton, A.; Petreanu, L. T.; Lansford, R.; Alvarez-Buylla, A.; Lledo, P.-M. Becoming a new neuron in the adult olfactory bulb. *Nat. Neurosci.* **2003**, *6*, 507–518.
- (94) Wadiche, L. O.; Bromberg, D. A.; Bensen, A. L.; Westbrook, G. L. GABAergic signaling to newborn neurons in dentate gyrus. *J. Neurophysiol.* **2005**, *94*, 4528–4532.
- (95) Scopa, C.; Marrocco, F.; Latina, V.; Ruggeri, F.; Corvaglia, V.; La Regina, F.; Ammassari-Teule, M.; Middei, S.; Amadoro, G.; Meli, G.; et al. Impaired adult neurogenesis is an early event in Alzheimer's disease neurodegeneration, mediated by intracellular  $\text{A}\beta$  oligomers. *Cell Death Differ.* **2020**, *27*, 934–948.
- (96) Moreno-Jiménez, E. P.; Flor-García, M.; Terreros-Roncal, J.; Rábano, A.; Cafini, F.; Pallas-Bazarrá, N.; Ávila, J.; Llorens-Martín, M. Adult hippocampal neurogenesis is abundant in neurologically healthy subjects and drops sharply in patients with Alzheimer's disease. *Nat. Med.* **2019**, *25*, 554–560.
- (97) Ziabreva, I.; Perry, E.; Perry, R.; Minger, S. L.; Ekonomou, A.; Przyborski, S.; Ballard, C. Altered neurogenesis in Alzheimer's disease. *J. Psychosom. Res.* **2006**, *61*, 311–316.
- (98) Perry, E. K.; Johnson, M.; Ekonomou, A.; Perry, R. H.; Ballard, C.; Attems, J. Neurogenic abnormalities in Alzheimer's disease differ between stages of neurogenesis and are partly related to cholinergic pathology. *Neurobiol. Dis.* **2012**, *47*, 155–162.
- (99) Martorana, A.; Koch, G. Is dopamine involved in Alzheimer's disease? *Front. Aging Neurosci.* **2014**, *6*, 252.
- (100) Mufson, E. J.; Counts, S. E.; Perez, S. E.; Ginsberg, S. D. Cholinergic system during the progression of Alzheimer's disease: therapeutic implications. *Expert Rev. Neurother.* **2008**, *8*, 1703–1718.
- (101) Rudy, C. C.; Hunsberger, H. C.; Weitzner, D. S.; Reed, M. N. The role of the tripartite glutamatergic synapse in the pathophysiology of Alzheimer's disease. *Aging Dis.* **2015**, *6*, 131.
- (102) Meltzer, C. C.; Smith, G.; DeKosky, S. T.; Pollock, B. G.; Mathis, C. A.; Moore, R. Y.; Kupfer, D. J.; Reynolds, C. F. Serotonin in aging, late-life depression, and Alzheimer's disease: the emerging role of functional imaging. *Neuropsychopharmacology* **1998**, *18*, 407–430.
- (103) Kalaria, R.; Andorn, A.; Tabaton, M.; Whitehouse, P.; Harik, S.; Unnerstall, J. Adrenergic receptors in aging and Alzheimer's disease: increased  $\beta 2$ -receptors in prefrontal cortex and hippocampus. *J. Neurochem.* **1989**, *53*, 1772–1781.
- (104) Tritsch, N. X.; Sabatini, B. L. Dopaminergic modulation of synaptic transmission in cortex and striatum. *Neuron* **2012**, *76*, 33–50.
- (105) Kuo, M.-F.; Paulus, W.; Nitsche, M. A. Boosting focally-induced brain plasticity by dopamine. *Cereb. Cortex* **2008**, *18*, 648–651.
- (106) Monte-Silva, K.; Kuo, M.-F.; Thirugnanasambandam, N.; Liebetanz, D.; Paulus, W.; Nitsche, M. A. Dose-dependent inverted U-shaped effect of dopamine (D2-like) receptor activation on focal and nonfocal plasticity in humans. *J. Neurosci.* **2009**, *29*, 6124–6131.
- (107) Jung, J. H.; An, K.; Kwon, O. B.; Kim, H.-s.; Kim, J.-H. Pathway-specific alteration of synaptic plasticity in Tg2576 mice. *Mol. Cells* **2011**, *32*, 197–201.
- (108) Jacobsen, J. S.; Wu, C.-C.; Redwine, J. M.; Comery, T. A.; Arias, R.; Bowlby, M.; Martone, R.; Morrison, J. H.; Pangalos, M. N.; Reinhart, P. H.; Bloom, F. E. Early-onset behavioral and synaptic deficits in a mouse model of Alzheimer's disease. *Proc. Natl. Acad. Sci. U.S.A.* **2006**, *103*, 5161–5166.
- (109) Chapman, P. F.; White, G. L.; Jones, M. W.; Cooper-Blacketer, D.; Marshall, V. J.; Irizarry, M.; Younkin, L.; Good, M. A.; Bliss, T.; Hyman, B. T.; et al. Impaired synaptic plasticity and learning in aged amyloid precursor protein transgenic mice. *Nat. Neurosci.* **1999**, *2*, 271–276.
- (110) Masters, M. C.; Morris, J. C.; Roe, C. M. "Noncognitive" symptoms of early Alzheimer disease: a longitudinal analysis. *Neurology* **2015**, *84*, 617–622.
- (111) Himeno, E.; Ohyagi, Y.; Ma, L.; Nakamura, N.; Miyoshi, K.; Sakae, N.; Motomura, K.; Soejima, N.; Yamasaki, R.; Hashimoto, T. Apomorphine treatment in Alzheimer mice promoting amyloid- $\beta$  degradation. *Ann. Neurol.* **2011**, *69*, 248–256.
- (112) Pan, Y.; Chen, X. Y.; Zhang, Q. Y.; Kong, L. D. Microglial NLRP3 inflammasome activation mediates IL-1 $\beta$ -related inflammation in prefrontal cortex of depressive rats. *Brain Behav. Immun.* **2014**, *41*, 90–100.
- (113) Gustin, A.; Kirchmeyer, M.; Koncina, E.; Felten, P.; Losciuto, S.; Heurtaux, T.; Tardivel, A.; Heuschling, P.; Dostert, C. NLRP3 Inflammasome Is Expressed and Functional in Mouse Brain Microglia but Not in Astrocytes. *PLoS One* **2015**, *10*, No. e0130624.
- (114) Lizzul, P. F.; Aphale, A.; Malaviya, R.; Sun, Y.; Masud, S.; Dombrovskiy, V.; Gottlieb, A. B. Differential expression of phosphorylated NF- $\kappa$ B/RelA in normal and psoriatic epidermis and downregulation of NF- $\kappa$ B in response to treatment with etanercept. *J. Invest. Dermatol.* **2005**, *124*, 1275–1283.
- (115) Irrera, N.; Vaccaro, M.; Bitto, A.; Pallio, G.; Pizzino, G.; Lentini, M.; Arcoraci, V.; Minutoli, L.; Scuruchi, M.; Cutroneo, G.; Anastasi, G. P.; Ettari, R.; Squadrato, F.; Altavilla, D. BAY 11-7082 inhibits the NF- $\kappa$ B and NLRP3 inflammasome pathways and protects against IMQ-induced psoriasis. *Clin. Sci.* **2017**, *131*, 487–498.
- (116) Kim, M. J.; Kim, H.; Cha, I. J.; Park, J. S.; Shon, J. H.; Liu, K. H.; Shin, J. G. High-throughput screening of inhibitory potential of nine cytochrome P450 enzymes in vitro using liquid chromatography/tandem mass spectrometry. *Rapid Commun. Mass Spectrom.* **2005**, *19*, 2651–2658.
- (117) Irwin, J. J.; Sterling, T.; Mysinger, M. M.; Bolstad, E. S.; Coleman, R. G. ZINC: a free tool to discover chemistry for biology. *J. Chem. Inf. Model.* **2012**, *52*, 1757–1768.
- (118) MOE, M. O. E. *Molecular Operating Environment*; Chemical Computing Group ULC: 1010 Sherbooke St. West, Suite #910, Montreal, QC, Canada, H3A 2R7, 2020.
- (119) Huang, J.; MacKerell, A. D., Jr. CHARMM36 all-atom additive protein force field: validation based on comparison to NMR data. *J. Comput. Chem.* **2013**, *34*, 2135–2145.
- (120) Yu, W.; He, X.; Vanommeslaeghe, K.; MacKerell, A. D., Jr. Extension of the CHARMM General Force Field to sulfonyl-containing compounds and its utility in biomolecular simulations. *J. Comput. Chem.* **2012**, *33*, 2451–2468.
- (121) Bussi, G.; Donadio, D.; Parrinello, M. Canonical sampling through velocity rescaling. *J. Chem. Phys.* **2007**, *126*, No. 014101.
- (122) Essmann, U.; Perera, L.; Berkowitz, M. L.; Darden, T.; Lee, H.; Pedersen, L. G. A smooth particle mesh Ewald method. *J. Chem. Phys.* **1995**, *103*, 8577–8593.
- (123) Abraham, M. J.; Murtola, T.; Schulz, R.; Páll, S.; Smith, J. C.; Hess, B.; Lindahl, E. GROMACS: High performance molecular simulations through multi-level parallelism from laptops to supercomputers. *SoftwareX* **2015**, *1-2*, 19–25.
- (124) Humphrey, W.; Dalke, A.; Schulten, K. VMD: visual molecular dynamics. *J. Mol. Graphics* **1996**, *14*, 33–38. 27–38.